Computers & Industrial Engineering 217 (2026) 112026

Contents lists available at ScienceDirect

Computers & Industrial Engineering

journal homepage: www.elsevier.com/locate/caie

Aging-aware fleet management for electric vehicle routing problem

Hadis Mohammadi [a,*], Eero Immonen [b], Mohsen Heydarzadeh [b], Juha Plosila [a], Hashem Haghbayan [a]

[a] Department of Computing, University of Turku, Turku 20500, Finland
[b] Computational Engineering and Analysis Research Group, Turku University of Applied Sciences, Turku 20520, Finland

ARTICLE INFO

Keywords:
Electric vehicle routing
Battery state of charge
Battery state of health
Aging-aware path planning

ABSTRACT

The Electric Vehicle Routing Problem (EVRP) is a key optimization challenge in autonomous and electric transportation. Unlike traditional routing, EVRP must consider battery constraints such as limited capacity and charging needs. Although routing methods have advanced, the integration of battery aging using realistic models remains underdeveloped. Addressing these dynamics is essential for improving long-term fleet efficiency. In this paper, we present a real-time, reconfigurable battery model that captures aging effects by updating key internal parameters based on the battery's current State of Charge (SoC) and State of Health (SoH). Using this model, we formulate a multi-objective optimization problem and develop a genetic algorithm that balances energy efficiency, battery lifespan, and quality of service. Results show that incorporating aging-aware battery dynamics significantly extends battery life and reduces operational costs.

1. Introduction

In 2022, the transportation sector was responsible for roughly 20% of global energy-related CO_2, ranking as the second-largest contributor after the power industry. Achieving climate targets requires a significant reduction in emissions from this sector, with a 25% decrease needed by 2030 (Agency, 0000). Electric vehicles (EVs) offer a solution to reduce environmental impact, as they have a significantly smaller ecological footprint compared to conventional internal combustion engine vehicles. EVs are particularly well-suited for urban logistics because they are more energy-efficient at low speeds, operate quietly, require less maintenance, and produce no greenhouse gas emissions during operation (İslim & Çatay, 2024). This has led to a surge in demand for EVs, positioning them as a sustainable alternative to traditional transportation methods (Tetik Kollugil et al., 2025).

The introduction of electric batteries creates new challenges for resource management, stemming from production and battery-related constraints. While EVs cut use-phase emissions, battery manufacturing carries notable greenhouse gas impacts (Xiao et al., 2025). Battery degradation further drives resource depletion, toxic waste, and health risks (Mrozik et al., 2021), and batteries still account for nearly 40% of vehicle cost (König et al., 2021). Therefore, extending battery life is critical for both cost and sustainability: poor handling accelerates degradation, prompting premature replacement and additional environmental burden (Li et al., 2025). This motivates incorporating battery health into operation planning to extend lifespan (İslim & Çatay, 2024); accordingly, several studies have begun to integrate aging into routing decisions (İslim & Çatay, 2024; Li et al., 2022; Longhitano et al., 2024; Perger & Auer, 2020; Xu et al., 2021; Zeng et al., 2022). Most EVRP studies treat SoC either as equivalent to energy, ignore the dependence of internal battery parameters on SoH and driving conditions, decouple routing from motion decisions that shape the SoC trajectory, fail to update battery parameters in real time as degradation accumulates, or use overly simplified models for charging periods. Addressing EV battery challenges, such as limited driving range, battery SoC, and degradation, requires accurate modeling of battery behavior and usage. Such models are especially important when applying optimization algorithms in mission planning.

This work presents a battery-aging-aware routing algorithm that integrates runtime battery dynamics to address the multi-objective optimization of delay, degradation, and energy consumption in electric vehicle fleets. By coupling a Genetic Algorithm (GA) with Local Search (LS), yielding the hybrid GALS method, the proposed evolutionary framework progressively updates the battery's SoH during optimization, moving beyond conventional static models, to enable aging-aware routing and motion planning. As demonstrated in the experimental section, assuming a non-progressive and static SoH during optimization leads to inaccurate estimation of battery health with respect to its actual value, and consequently results in a suboptimal path plan. To address this issue, we develop a genetic-algorithm-based evolutionary framework in which, at each iteration, the SoH is updated using the

* Corresponding author at: Department of Computing, University of Turku, Turku 20500, Finland.
E-mail address: hmokam@utu.fi (H. Mohammadi).

https://doi.org/10.1016/j.cie.2026.112026
Received 3 April 2025; Received in revised form 3 February 2026; Accepted 7 April 2026
Available online 8 April 2026

current value of the battery SoC, which is first estimated through an run time Electrical Equivalent Circuit Model (EECM). While the convergence and efficiency of genetic-based algorithm have been studied previously (Karakatič, 2021; Liu et al., 2024), we focus here on how this optimizer solves the EVRP problem while explicitly considering nonlinear, reconfigurable battery dynamics. Our joint aging-aware optimization simultaneously optimizes path selection, vehicle speed, acceleration, and partial charging while updating SoC and SoH at runtime, allowing internal battery parameters to evolve during operation and capturing the real-time impact of degradation on performance and cost. Charging time is also modeled as a nonlinear function that accounts for SoH effects.

The main contributions of this work can be summarized as follows:

- We formulate the EVRP with Aging-Aware Fleet Management (EVRP-AFM), a framework that integrates battery dynamics to perform multi-objective optimization of delay, energy consumption, and battery degradation through the joint optimization of routing, speed, acceleration, and partial charging as decision variables.
- We propose a runtime-reconfigurable battery modeling approach where internal parameters are updated online using the instantaneous SoC and SoH. Battery SoH is estimated via a cycle-decomposition method applied to the SoC trajectory, while charging duration is formulated as a nonlinear function of the SoH.
- We validate the proposed EVRP-AFM method through extensive experiments, analyzing how different optimization criteria impact battery lifespan, operational cost, and the resulting routing and motion decisions.

The remainder of this paper is organized as follows: Section 2 provides a literature review, highlighting the significance of our contribution by briefly discussing battery and degradation models in EVRP. Section 3 introduces the mixed-integer programming formulation of EVRP-AFM. Section 4 details the battery model and the dynamic behavior of the vehicle. Section 5 presents the optimization algorithm and its framework. Section 6 validates the proposed method through experimental results. Finally, Section 7 summarizes the findings and concludes the paper.

2. Literature review

Recent research on the EVRP has extended the classical Vehicle Routing Problem (VRP) framework (Braekers et al., 2016) by incorporating constraints specific to EVs. In contrast to the conventional VRP, where vehicles are powered by internal combustion engines, the EVRP considers vehicles powered by electrical batteries. This modification introduces new challenges for routing and resource management, arising from battery-related constraints such as limited driving range, battery SoC, and battery degradation (Longhitano et al., 2024). These challenges are closely linked to accurate modeling of battery behavior and usage, which is crucial when applying optimization algorithms throughout the mission planning process. Battery modeling has therefore become a central aspect of EVRP research. However, many existing studies adopt simplified battery representations, typically focusing only on basic SoC or SoH evolution and simplified charging behavior (İslim & Çatay, 2024; Shehabeldeen et al., 2023; Wei et al., 2025; Yu et al., 2025). Such simplified approaches can limit the effectiveness of battery-aware optimization, as they do not fully capture the complex and nonlinear behavior of real batteries. Among recent state-of-the-art studies, some works have begun to model battery behavior and usage in detail. In the following, we categorize these studies into three main groups and discuss each in detail: (1) approaches that model vehicle motion dynamics and their impact on battery energy consumption; (2) battery modeling approaches that estimate battery SoC and SoH; and (3) studies that focus on modeling the charging periods. A summary of the state-of-the-art comparisons, organized according to this categorization, is presented in Table 1.

2.1. Energy consumption model

Modeling the mechanical energy consumption of EVs is essential for the EVRP, as it directly determines the battery charging level and route feasibility. Most studies use distance-based models, where energy consumption is assumed to be a linear function of travel distance (Ceselli et al., 2021; He et al., 2025; İslim & Çatay, 2024; Wei et al., 2025; S. Yang et al., 2025; Yu et al., 2025; Zang et al., 2022). This approach is popular because it is computationally efficient for complex routing problems. Some studies use an even simpler method by assigning fixed, pre-computed energy values to each road segment (Pelletier et al., 2018). Although these models are easy to implement, they ignore important real-world driving factors such as speed variation, acceleration, road gradient, aerodynamic drag, and vehicle load. As a result, the planned routes may be infeasible in practice because the simplified modeling assumptions do not accurately reflect the actual energy consumption and battery behavior during real-world vehicle operation (Pelletier et al., 2017). To improve accuracy, another group of studies uses motion dynamics models to calculate mechanical energy consumption directly and estimate the battery state of charge. The level of detail in these models varies. Some assume constant vehicle speed to reduce complexity (Futalef et al., 2023; Jung, 2025; Ma et al., 2021; Perger & Auer, 2020; Romet et al., 2021; Xiao et al., 2019; B. Yang et al., 2025). Others model instantaneous power demand and consider detailed factors such as speed profiles, acceleration (Barco et al., 2017; Basso et al., 2019; Erdelić et al., 2025; Fan et al., 2025; Houalef et al., 2025). However, many of these state-of-the-art approaches still rely on simplified assumptions or do not fully capture the realistic, nonlinear behavior of battery dynamics, which can limit their applicability in practical EV routing scenarios.

2.2. Battery model

In this subsection, we review state-of-the-art studies on battery modeling in the EVRP by considering two main categories of modeling the battery SoC and SoH as is explained in the following.

2.2.1. Battery SoC modeling

Two main categories are used to model SoC in battery-constrained EVRP problems. The first and most commonly used category treats SoC and energy consumption of the EV as equivalent. In this approach, energy consumption is directly used to represent the decrease in SoC. These studies rely on different energy consumption models for the EV, including distance-based and motion dynamics models, as discussed in the previous section (Barco et al., 2017; Basso et al., 2019; Ceselli et al., 2021; Erdelić et al., 2025; He et al., 2025; İslim & Çatay, 2024; Jung, 2025; B. Yang et al., 2025; S. Yang et al., 2025; Yu et al., 2025; Zang et al., 2022). However, this method is less robust than explicitly constraining SoC and may lead to infeasible routes in practice. Besides the lack of accuracy, which is the main cause of the routing algorithm's lack of robustness, the model also assumes a constant terminal battery voltage. This assumption limits its applicability, as it does not hold for many battery types or operating conditions (Longhitano et al., 2024). Some other studies in this category do not explicitly describe how SoC variation or energy consumption is modeled. Instead, they assume that the energy required is known in advance (Froger et al., 2022, 2019; Goeke, 2019; Karakatič, 2021). None of these studies consider a realistic battery SoC model, as they do not account for the dynamic characteristics of the battery throughout the task duration. Such realism is crucial for accurately capturing battery behavior in EVPR problems (Pelletier et al., 2017).

The second category of studies adopt more realistic battery SoC modeling approaches. These studies explicitly model battery behavior and dynamics rather than approximating SoC through energy consumption alone. A common method within this category is the use of an EECM. For example, Longhitano et al. (2024) addresses the EVRP using

Table 1
A comparison of our proposed approach with existing studies in the EVRP that incorporate battery characteristics.

References	Non-linear charging period with SoH effect	Energy consumption model		Battery model	
		Motion model with dynamic speed	Motion model with constant speed	SoH estimation with Cycle decomposition	SoC estimation with run-time battery model
Ceselli et al. (2021), He et al. (2025), İslim and Çatay (2024), Schiffer et al. (2021), Shehabeldeen et al. (2023), Wei et al. (2025), S. Yang et al. (2025), Yu et al. (2025), Zang et al. (2022) and Zhou et al. (2025)	×	×	×	×	×
Barco et al. (2017), Basso et al. (2019), Erdelić et al. (2025), Fan et al. (2025), Houalef et al. (2025) and Longhitano et al. (2024)	×	✓	×	×	×
Futalef et al. (2023), Jung (2025), Ma et al. (2021), Perger and Auer (2020), Romet et al. (2021), Xiao et al. (2019) and B. Yang et al. (2025)	×	×	✓	×	×
Longhitano et al. (2024)	×	✓	×	✓	×
Ours	✓	✓	×	✓	✓

a relatively realistic SoC model based on EECM, which accounts for battery dynamics and operational driving factors. However, although this study employs a dynamic SoC, it assumes that the battery EECM parameters remain fixed during vehicle operation, which is still far from a realistic assumption. In real battery operation, both the SoC and SoH are highly dynamic and have a significant impact on battery characteristics; therefore, they must be considered when modeling batteries for routing problems. In contrast to these approaches, the reconfigurable model employed in this paper incorporates runtime updates of battery parameters based on ongoing SoC and SoH estimation. We demonstrate that such runtime reconfiguration leads to a more realistic battery model and enables more efficient routing decisions.

2.2.2. Battery SoH modeling

The SoH is defined as the ratio of the battery's actual capacity to its nominal capacity, and it decreases nonlinearly over time due to internal electrochemical reactions (Li & Xue, 2025; Liu et al., 2023). In EVRP studies that account for battery degradation, SoH is typically modeled using one of three approaches: Simplistic, semi-empirical, or cycle decomposition models. Simplified models use coarse approximations, such as linear annual capacity loss (Schiffer et al., 2021), constant degradation rates derived from average usage (Shehabeldeen et al., 2023), or capacity fade proportional to the number of charge cycles (Jung, 2025).

Semi-empirical models are the most commonly used approach in decision-making problems. These models combine model-based methods (Ahmed et al., 2025; Longhitano et al., 2024) with data-driven approaches (Mu et al., 2025; Wang et al., 2021). They avoid detailed electrochemical modeling and require less data (Zhang et al., 2017; Zhao et al., 2019). They estimate degradation using stress factors related to vehicle use, such as Depth of Discharge (DoD), average value of SoC, and charging rates (Barré et al., 2013; Yu et al., 2025), making them the most practical choice for EVRP frameworks. For example, several studies estimate Wear Cost (WC) by mapping DoD to cycle life and accumulating degradation over SoC intervals (Azadeh et al., 2022; Guo et al., 2022; İslim & Çatay, 2024; S. Yang et al., 2025; Zeng et al., 2022; Zhou et al., 2022). Other studies extend this framework by incorporating SoC ranges and cycling data into WC functions (Xu et al., 2021), or by including temperature effects and average SoC impacts (Barco et al., 2017). Further variants estimate capacity fade via SoC profile statistics (Saner et al., 2022), focus on minimizing cumulative energy flow (Perger & Auer, 2020), or apply DoD-linked WC to both charging and discharging phases (Pelletier et al., 2018).

Simplified and semi-empirical models, despite their simple implementation and light-weight calculation, are often too general and insufficiently detailed, may not fully capture degradation from real EV driving cycles, and typically ignore opportunistic energy recoveries such as regenerative braking. An alternative approach is cycle decomposition modeling, which overcomes these limitations by explicitly tracking recurring charge–discharge patterns. For instance, methods such as the Rainflow Counting algorithm decompose SoC histories into individual cycles (Ghanaee et al., 2025; Nebuloni et al., 2025; Xu et al., 2016), which can then be used to estimate the SoH during vehicle operation. This cycle decomposition enables more accurate degradation estimation under varying driving conditions and dynamic motion factors that are often neglected in simpler SoH models. Recent EVRP study (Longhitano et al., 2024) demonstrate how this approach can better account for real-world driving cycles and energy recovery events. In this study, we also use the Rainflow cycle decomposition method.

2.3. Charging period

A large body of research investigates battery charging behavior during vehicle routing optimization. These studies can be broadly categorized based on how the charging period is modeled during the EVRP optimization. Some studies assume that the battery charging time is linearly proportional to its charging rate (Erdelić et al., 2025; Fan et al., 2025; J. Li et al., 2025; Yuan et al., 2026). While such linear charging models are computationally simple, they are inherently unrealistic due to ignorance of the concave nature of SoC charging trajectories while SoC is high (approximately higher than 50%). This leads to routing decisions with results in inaccurate charging stops for the EV, which might result in destruction of total EV schedule process (Montoya et al., 2017). Several studies model charging time as a nonlinear process and approximate it using piecewise charging models (Futalef et al., 2023;

Table 2
Table of variables and inputs in this work.

Inputs		Variables	
Symbol	Description	Symbol	Description
N	Set of customers	R^z	Mission route for vehicle z
S	Set of charging stations (CS)	R_q^z	qth node in mission route
Z	The fleet of EVs	t_q^z	Arrival time at node q
n	Number of customers	t_0^z	Mission start time decision variable
l	Number of CSs	C_q^z	Vehicle load at node q
$[y^-, y^+]$	Customer time window	SoC_k	State of Charge at time step k
D	Customer demand	SoH_k	State of Health at time step k
W	Maximum allowed vehicle payload	f	Amount of charge decision variable
$\Gamma(.)$	Charging time	a_{max}^z	Vehicle maximum acceleration decision variable
$V_{max,road}$	Road maximum speed	V_{max}^z	Vehicle maximum speed decision variable
ρ_{air}	Air density	V_{oc}	Open-circuit voltage
C_r	Rolling resistance	I	Battery Current
C_w	Drag coefficient	V_{tgt}	Target speed
A	Vehicle frontal area	$e_{R_qR_{q+1}}$	Energy consumption between two nodes
α	Inclination angle	$Cyc_{(SoC)}$	Number of SoC cycles
m	Total vehicle mass	n_i	Cycle type
T_s	Sampling time	S_{σ_i}	Stress coefficients related average SoC
C_{init}	Battery nominal capacity	S_{δ_i}	Stress coefficients related Depth of Discharge (DoD)
		S_{T_i}	Stress coefficients related temperature
j_a	Number of acceleration options		
j_v	Number of speed options		

Guo et al., 2022; Karakatič, 2021; Kim & Do Chung, 2023; Zhou et al., 2022). These works capture the aforementioned nonlinear charging behavior by partitioning the charging period into multiple segments and defining a linear model for each segment. When combined, these segments approximate the true nonlinear charging behavior with an acceptable level of fidelity. However, these approaches typically neglect the impact of battery SoH during the charging process. This omission is important, as each electric vehicle experiences a distinct degree of battery degradation, which directly affects charging time. To address this limitation, this paper adopts the piecewise charging framework while explicitly incorporating the effect of SoH on charging time. We demonstrate that accounting for SoH significantly improves the accuracy of battery charging process modeling.

3. Problem statement

This section describes the mathematical formulation of the EVRP-AFM, emphasizing optimization of delivery processes for EVs while accounting for battery degradation and aging effects. Table 2 summarizes the input data and variables used in the formulation. The mission's mechanical and battery characteristics are updated at every sampling interval T_s; the index k counts these successive updates, so a subscript "k" denotes the value after the kth update.

In this problem, the fleet of EVs is represented as a set Z, where each element $z \in Z$ corresponds to a specific vehicle responsible for delivering goods to various customers. Each customer has a specific time window which they need to receive their delivery. The key constraints of the EVRP are that every customer must be visited exactly once, each EV must operate within its battery capacity limits, and all EVs must begin and end their routes at the depot. The primary goal is to minimize a combined cost that includes both battery degradation and operational expenses, while ensuring that all constraints are satisfied. In this study, we define a network denoted as $G = (V, E)$, where $V = \{0\} \cup N \cup S$ represents a set of nodes, including the depot, customers, and Charging Stations (CS). The set $N = \{1, 2, \dots, n\}$ denotes the n customer nodes, while $S = \{n+1, n+2, \dots, n+l\}$ represents the l nodes corresponding to the available CS. The set of arcs $E = \{(i, j) : i, j \in V, i \neq j\}$ represents possible directed connections between the nodes within the network.

The mission route of the EV_z is defined as:

$$R^z = [R_0^z, R_1^z, \dots, R_{r-1}^z]^T \tag{1}$$

where the sequence of nodes visited by vehicle z, including customers and CSs, is denoted by R^z. Specifically, R_q^z represents the qth node visited by EV_z during its mission, where r indicates the length of the mission, and both R_0^z and R_{r-1}^z are the depot. The service requested by customer $i \in N$ is defined by the time window $[y_i^-, y_i^+]$ and the package mass $D_i > 0$. The maximum payload capacity of an EV_z is denoted by W, and the mass variation after delivering the package to node $R_q^z \in N$ is given by $D_{R_q^z}$, where it is zero if the node is a CS. Let C_{q+1}^z represent the load carried by vehicle z when it arrives at node $q+1$:

$$C_{q+1}^z = \begin{cases} C_q^z - D_{R_q^z}, & \text{if } R_q^z \in N, \\ C_q^z, & \text{if } R_q^z \in S. \end{cases} \tag{2}$$

The arrival time at node $q+1$ is computed by adding the travel time from node q to node $q+1$, starting from the initial mission time t_0^z.

$$t_{q+1}^z = \begin{cases} t_q^z + t_{R_q^z R_{q+1}^z}, & \text{if } R_q^z \in N, \\ t_q^z + \Gamma\left(SoC_k, SoH_k, f_{R_q^z}\right) + t_{R_q^z R_{q+1}^z}, & \text{if } R_q^z \in S. \end{cases} \tag{3}$$

In Eq. (3), function Γ represents the time required at the node R_q^z to charge the vehicle, which is determined by its SoC, SoH at time step k, along with the amount of charge $f_{R_q^z}$. The problem is formulated with the following decision variables: the sequence of nodes visited by each EV, $R = [R^1, \dots, R^z]^T$; the charging plan $F = [F^1, \dots, F^z]^T$, where $F^z = [f_{R_0^z}, \dots, f_{R_{r-1}^z}]$ represents the amount of charge received at $R_q^z \in S$ along the route; the maximum acceleration $a_{\max} = [a_{\max}^1, \dots, a_{\max}^z]^T$; the maximum velocity $V_{\max} = [V_{\max}^1, \dots, V_{\max}^z]^T$; and the departure time $t_0 = [t_0^1, \dots, t_0^z]^T$, which specifies when each EV begins its mission. The vehicle control parameters $(a_{\max}, V_{\max})$ define the permissible acceleration and speed ranges for each vehicle and can be adjusted remotely to optimize performance.

The mission planning cost function (Eq. (4)) comprises three components, each influenced by specific decision variables. The coefficients ω_1, ω_2, and ω_3 quantify the relative priority weights associated with delivery delay, battery degradation, and total energy consumption, respectively. In line with previous study (Sun et al., 2024), we reformulate the multi-objective optimization problem as a single-objective one using weighted coefficients that encode user preferences among the objectives. While the Pareto frontier is a widely adopted approach for multi-objective optimization through the generation of non-dominated solutions, its direct application can be computationally intensive despite its theoretical suitability for the problem considered. This challenge is particularly evident in large-scale scenarios and in problems involving complex system dynamics, and becomes more pronounced as

the number of objectives increases (Mattson & Messac, 2005). The computational burden is further exacerbated when additional optimization components, such as battery SoC and SoH estimation, are embedded within the evolutionary optimization process, resulting in increased runtime. In the proposed method, the weights of the normalized objective functions are specified by the user according to strategic priorities, yielding a single optimized solution rather than an entire Pareto set. This formulation significantly reduces computational cost while preserving flexibility in expressing objective preferences. By adjusting the weights to reflect optimization priorities and environmental conditions, the proposed approach maintains adaptability and solution diversity while substantially reducing algorithmic complexity.

$$C(R,F,t_0,V_{\max},a_{\max}) = \underbrace{\omega_1 \sum_{z\in Z}\sum_{q=0}^{r^z} \max\left((y^-_{R^z_q} - t^z_{R^z_q}),0\right) + \max\left((t^z_{R^z_q} - y^+_{R^z_q}),0\right)}_{\text{Total delays}} + \omega_2 \underbrace{\sum_{z\in Z} \Delta SoH}_{\text{Total degradation}} + \omega_3 \underbrace{\sum_{z\in Z}\sum_{q=0}^{r^z} e_{R^z_q R^z_{q+1}}}_{\text{Total energy consumption}} \tag{4}$$

Here, ΔSoH_k denotes the battery health drop at step k; the accumulated degradation up to step k is computed from the SoC trajectory $\text{SoC}_{0:k}$, with details provided in Section 4.2.

$$\Delta SoH_k = SoH(SoC_{0:k-1}) - SoH(SoC_{0:k}) \tag{5}$$

The objective is to find a set of optimal routes R^* for all vehicles, along with a^*_{max}, V^*_{max}, F^*, and t^*_0 such that the cost function (6) is minimized while satisfying the constraints (7)–(17):

$$\min_{R^*,F^*,t^*_0,V^*_{\max},a^*_{\max}} C(R,F,t_0,V_{\max},a_{\max}) \tag{6}$$

$$\sum_{z\in Z}\sum_{q=1}^{r_{z-2}} \delta(R^z_q,i) = 1, \quad \forall i \in N, \quad R^z_q \in N \tag{7}$$

$$\sum_{i\in N}\sum_{z\in Z}\sum_{q=1}^{r_{z-2}} \delta(R^z_q,i) = n, \quad R^z_q \in N \tag{8}$$

$$\sum_{q=0}^{r_{z-2}} \delta(R^z_q,0) = 1, \quad \forall z \in Z \tag{9}$$

$$\sum_{q=1}^{r_{z-1}} \delta(R^z_q,0) = 1, \quad \forall z \in Z \tag{10}$$

$$\sum_{q=1}^{r_{z-2}} \delta(R^z_q,c) \le 1, \quad \forall c \in C, \quad \forall z \in Z, \quad R^z_q \in C \tag{11}$$

$$\sum_{q=1}^{r_{z-2}} \delta((R^z_q,R^z_{q+1}),(i,j)) - \sum_{p=1}^{r_{z-2}} \delta((R^z_p,R^z_{p+1}),(j,i)) = 0, \quad \forall j,i \in V, \quad \forall z \in Z \tag{12}$$

$$SoC_{limit} \le \min SoC_k(SoH_k, power(a^z_{\max}, v^z_{\max}), T_s) \tag{13}$$

$$SoH_{limit} \le \min SoH_k(SoC) \tag{14}$$

$$\sum_{q=1}^{r_{z-2}} D_{R^z_q} \le W, \quad \forall z \in Z \tag{15}$$

$$a^z_{\max} \in [a_{\max,1}, a_{\max,2}, \dots, a_{\max,j_a}], \quad \forall z \in Z \tag{16}$$

$$V^z_{\max} \in [V_{\max,1}, V_{\max,2}, \dots, V_{\max j_v}], \quad \forall z \in Z \tag{17}$$

The indicator function $\delta(x,y)$ is defined as:

$$\delta(x,y) = \begin{cases} 1, & \text{if } x = y, \\ 0, & \text{otherwise.} \end{cases} \tag{18}$$

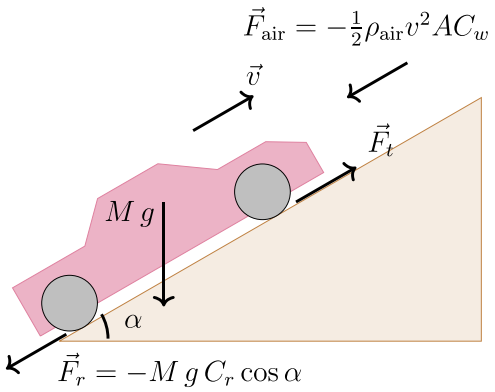

Fig. 1. Balance of forces acting on a vehicle on an incline, including gravitational, air resistance, rolling resistance, and driving forces.

Constraints (7) guarantee that each customer is visited exactly once by a vehicle, while Constraints (8) ensure that the total number of customer visits across all vehicles matches the number of customers. The depot-related requirements are covered by Constraints (9) and (10), ensuring that each vehicle starts and ends its route at the depot. In terms of visiting CS, Constraints (11) limit each vehicle to visiting any charging station at most once. Constraint (12) enforces flow conservation at each node, ensuring that the number of times a vehicle enters and exits a node is balanced. To ensure battery health and performance, Eqs. (13) and (14) impose limits on the vehicle's battery level and health. The SoC at time step k, is determined by the SoH, power consumption, dependent on maximum acceleration and velocity, and the sampling time. Constraint (15) ensures that the total customer demand assigned to a vehicle does not exceed its payload capacity. Lastly, Constraints (16) and (17) define the maximum acceleration and velocity for each vehicle, ensuring that the decision variables are selected from discrete catalogs. Specifically, $\{a_{\max,1},\dots,a_{\max,j_a}\}$ and $\{V_{\max,1},\dots,V_{\max,j_v}\}$ are the admissible discrete values for $a^z_{\max}$ and $V^z_{\max}$, respectively, where j_a and j_v are the numbers of discrete choices available.

The next section presents a model for estimating degradation for calculating ΔSoH and updating the SoC, incorporating the optimization variables that influence the decision-making problem.

4. Battery modeling and vehicle dynamics

In addressing the EVRP-AFM, we emphasize accurate modeling of battery and vehicle dynamics, incorporating road topography and the EV's speed and acceleration behaviors for a comprehensive analysis.

4.1. SoC estimation

To estimate battery degradation, the SoC profile must be determined. This requires first evaluating the vehicle's longitudinal dynamics by calculating the mechanical power required during operation. Fig. 1 depicts the forces acting on a moving vehicle. Using Newton's Second Law, the mechanical power (P_{mec}) at each time step k is calculated as:

$$P_{\text{mec},k} = V_k\left(\frac{\rho_{\text{air}} C_w A V_k^2}{2} + mg\sin(\alpha) + mg\cos(\alpha)C_r + ma\right) \tag{19}$$

where ρ_{air} is the air density, C_w is the drag coefficient, A is the frontal area of the vehicle, m is the total vehicle mass, g is the gravitational acceleration, α is the incline angle, C_r is the rolling resistance coefficient, a is the vehicle's acceleration, and V_k represents the vehicle's speed at the time step k.

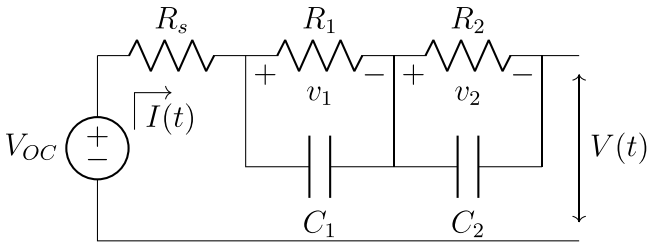

Fig. 2. Schematic diagram of second-order Electrical Equivalent Circuit Model (EECM).

In our research, we implement the second-order Electrical EECM, based on the model described in Heydarzadeh et al. (2023), to accurately estimate the SoC. This model, which we refer to as EECM-SoC-SoH, represents the internal dynamics of lithium-ion batteries, with internal parameters modeled as functions of degradation and SoC. By considering these factors, it provides a reliable framework for long-term SoC estimation.

Our work employs a run-time model to identify six EECM parameters affected by degradation, as illustrated in Fig. 2, under specific SoC and SoH conditions. The model estimates SoC by accounting for its dependency on SoH. The open-circuit voltage (V_{OC}) is modeled in Eq. (20) as a third-order polynomial of SoC combined with a first-order SoH term, using coefficients $p_0, \ldots, p_6$. Similarly, Eq. (21) defines the function F, which captures the relationship between SoC, SoH, and parameters like R_s, C_1, R_1, C_2, and R_2 using an exponential SoH term and a second-order polynomial in SoC with coefficients $a_{X,0}, \ldots, a_{X,4}$. In Fig. 2, R_s represents ohmic resistance, while R_1, C_1, R_2, and C_2 describe the parallel RC circuits.

$$V_{\mathrm{OC},k} = V(SoC_k, SoH_k; (p_0, \ldots, p_6)) \tag{20}$$

$$X_k = F(\mathrm{SoC}_k, \mathrm{SoH}_k; a_{X,0}, \ldots, a_{X,4}), \quad X \in \{R_s, C_1, R_1, C_2, R_2\} \tag{21}$$

By integrating the mechanical characteristics of the vehicle with the EECM, which accounts for the internal dynamic behavior of the battery, we can achieve a more realistic representation of battery performance.

The following set of equations models the battery system by capturing the relationships between mechanical power, electrical power, voltage dynamics, and SoC evolution:

$$P_{elec,k} = \beta P_{mec,k} \tag{22}$$

$$I_k = \frac{-\left(v_k^1 + v_k^2 - V_{\mathrm{OC},k}\right)}{2 \cdot R_{s,k}} \pm \frac{\sqrt{\left(v_k^1 + v_k^2 - V_{\mathrm{OC},k}\right)^2 - 4 \cdot R_{s,k} \cdot P_k^{elec}}}{2 \cdot R_{s,k}} \tag{23}$$

$$v_{k+1}^1 = \left(1 - \frac{T_s}{R_{1,k}C_{1,k}}\right) v_k^1 + \frac{T_s}{C_{1,k}} I_k \tag{24}$$

$$v_{k+1}^2 = \left(1 - \frac{T_s}{R_{2,k}C_{2,k}}\right) v_k^2 + \frac{T_s}{C_{2,k}} I_k \tag{25}$$

$$\mathrm{SoC}_{k+1} = \mathrm{SoC}_k - \frac{\eta T_s I_k}{C_{\mathrm{init}} \mathrm{SoH}_k} \tag{26}$$

Eq. (22) defines the relationship between the electrical power $P_{\mathrm{elec},k}$ and the mechanical power $P_{\mathrm{mec},k}$, scaled by an efficiency coefficient β, which is set to 1 for simplicity in this context. The battery current I_k is determined using Eq. (23). Eqs. (24) and (25) describe the voltage dynamics across the RC branches of the battery. The SoC evolution is captured in Eq. (26), with T_s denoting the sampling time interval. To effectively utilize these equations, it is essential to know the initial values of the SoH_0, SoC_0, initial current (I_0), and initial voltages across the RC branches (v_0^1 and v_0^2).

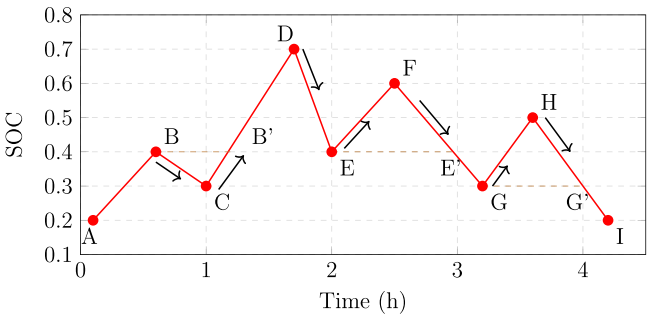

Fig. 3. Rainflow cycle counting process for an example SoC profile.

Table 3
Results of Rainflow cycle-decomposition, cycle type, depth, and average SoC.

Cycle	n_i	δ	σ
A-D	Half	0.499	0.449
B-C-B′	Full	0.100	0.350
D-I	Half	0.499	0.449
E-F-E′	Full	0.199	0.500
G-H-G′	Full	0.200	0.400

4.2. Aging model

To assess the impact of the mission plan on the SoH, we adopt a model based on Rainflow algorithm. This model analyzes the SoC profile to identify individual cycles and evaluate their contribution to battery degradation. Similar to the method described in Xu et al. (2016), we employ a cycle-counting approach where the average SoC, the amplitude of the cycles, and the cell temperature are the primary factors influencing the degradation function.

Fig. 3 and Table 3 illustrate an example of the Rainflow cycle-counting process applied to an SoC trajectory. This example highlights key parameters for each cycle, such as the average SoC (σ_i), cycle amplitude (δ_i), and the type of cycle (e.g., full or half). This paper focuses on cycle aging, which refers to the battery's capacity loss caused by repeated charging and discharging cycles. The degradation function, accounting for stress factors across all cycles, is expressed as:

$$f_d = \sum_{i=1}^{Cyc_{(SoC_{0:k})}} n_i S_{\sigma_i} S_{\delta_i} S_{T_i} \tag{27}$$

Here, $Cyc_{(SoC_{0:k})}$ is the total number of cycles for SoC profiles up to time step k, and n_i indicates whether cycle i is full or partial. The parameters σ_i, δ_i, and T_i denote the average SoC, DoD, and average cell temperature for cycle i, respectively. The stress factors for each cycle, adapted from Xu et al. (2016), are defined as:

$$\begin{aligned} S_{\sigma_i} &= e^{k_\sigma(\sigma_i - \sigma_{\mathrm{ref}})} \\ S_{T_i} &= e^{k_T(T_i - T_{\mathrm{ref}})\frac{T_{\mathrm{ref}}}{T}} \\ S_{\delta_i} &= \left(k_{\delta_1} {\delta_i}^{k_{\delta_2}} + k_{\delta_3}\right)^{-1} \end{aligned} \tag{28}$$

In these equations, S_{σ_i}, S_{δ_i}, and S_{T_i} are the stress factors related to the average SoC, cycle depth, and temperature, respectively. The terms T_{ref} and σ_{ref} denote the reference temperature and SoC. Additionally, k_σ, k_T, k_{δ_1}, k_{δ_2}, and k_{δ_3} are empirical constants. The final SoH at each time step is updated using the degradation function:

$$SoH_k = e^{-f_d} \tag{29}$$

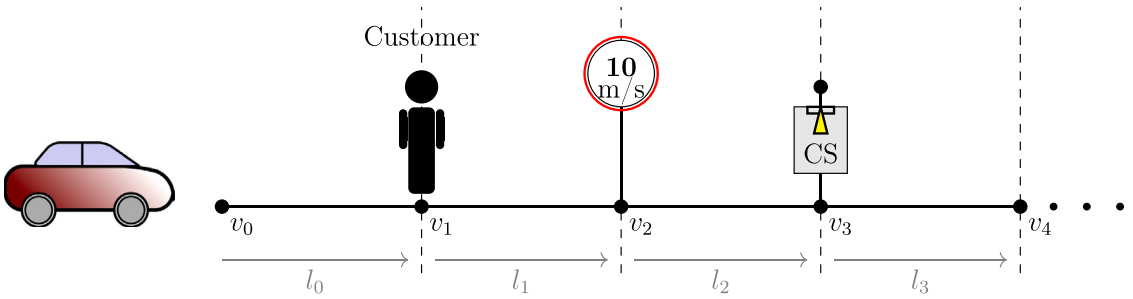

Fig. 4. Graph construction with nodes representing key points influencing speed and power: customer, speed limit, and charging station.

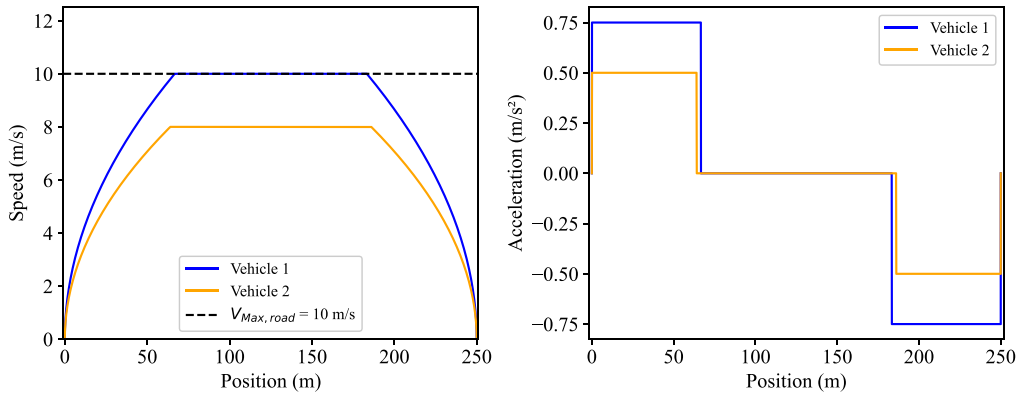

Fig. 5. Comparison of speed and acceleration profiles for two EVs. Vehicle 1, with a higher V^z_{max} and a^z_{max}, reaches a higher final velocity than Vehicle 2, both adhering to the road's maximum speed limit.

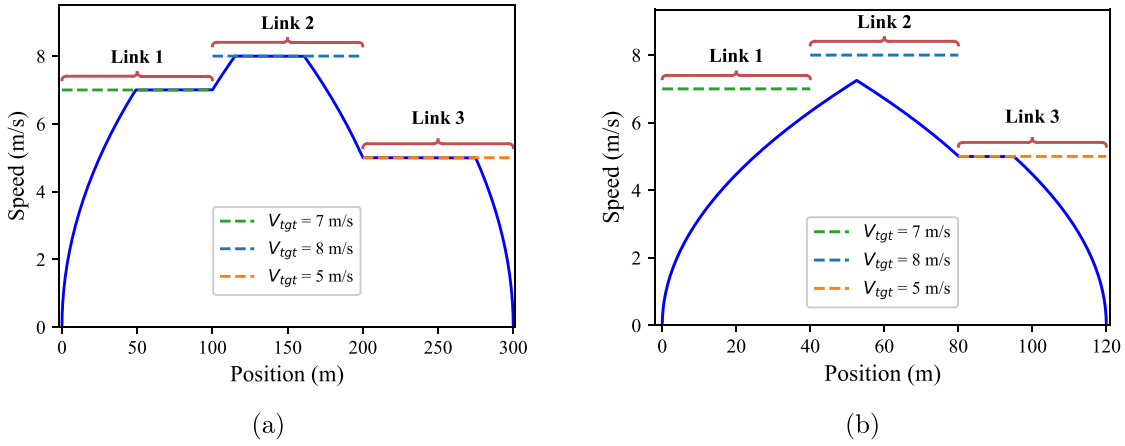

Fig. 6. Vehicle speed profiles: (a) consecutive road links, and (b) short consecutive road links.

4.3. Vehicle dynamics model

We enhance the EVRP-AFM by incorporating dynamic speed and acceleration profiles. This integration accounts for road topography providing a more realistic approach. Vehicles are assumed to accelerate at maximum rates until reaching speed limits as illustrated in 5. In our model, maximum speed and acceleration treated as optimization variables. These parameters, which can be adjusted remotely, directly influence the $P_{mec,k}$ and, consequently, the $P_{elec,k}$.

Building on the methodologies in Basso et al. (2019) and Longhitano et al. (2024), our approach models acceleration and braking dynamics, ensuring a more realistic representation of energy consumption and vehicle behavior. Using road data, we construct a road graph $G_r = (V_r, E_r)$, where the nodes represent key points that influence mechanical power, such as stop points, speed limit markers, slope variations and other key locations. Each node $v \in V_r$ in the road graph is defined as:

$$v_i = (\text{type}, V_{\max,road}, \theta, \text{coord}) \tag{30}$$

where type specifies the role of the node in the road network (e.g., stop point, or speed limit marker), $V_{\max,road}$ is the maximum speed for the road link, θ is the slope angle, and coord denotes the geographical coordinates of the node, and i is the node's unique ID in the graph. Fig. 4 shows an example of constructing a graph from road information based on a section of the environment.

After constructing the graph, the final velocity for each road segment is calculated as the minimum of the vehicle's maximum speed and the road segment's speed limit, as shown in Eq. (31):

$$V_{\text{tgt}} = \min(V^z_{\max}, V_{\max,\text{road}}) \tag{31}$$

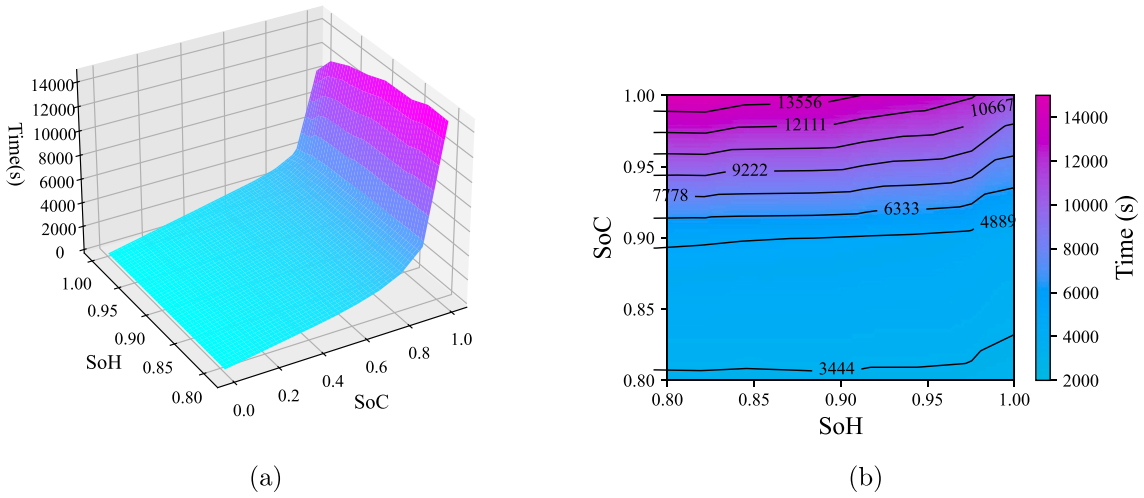

Fig. 7. Charging time by considering SoH. (a) 3D surface plot of charging time. (b) Contour map highlighting charging time regions.

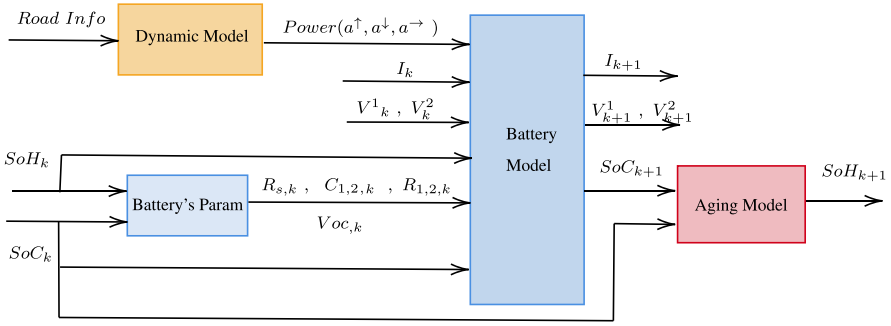

Fig. 8. Overall dynamic framework for SoH estimation.

Once the target speed V_{tgt} is established, the vehicle's acceleration ($a^{\uparrow}$), braking ($a^{\downarrow}$), or constant-speed movement ($a^{\rightarrow}$) can be determined based on the maximum allowable acceleration (a^{z}_{max}), the target speed, and the vehicle's position as specified in the mission plan (R_z).

Fig. 5 compares the speed and acceleration profiles of two EVs on a road segment, showing how their speed and acceleration vary with position under the influence of the road's maximum speed limit. Both vehicles decelerate and stop at the segment's end.

According to Basso et al. (2019), two specific scenarios are considered: when there are no stop points between consecutive road links, and when the links are short. In the first scenario, the EV adjusts its speed based on the road's speed limit, accelerating if the V_{tgt} increases between links and decelerating if it decreases. This behavior is illustrated in Fig. 6(a), which shows an EV starting from rest, accelerating on a link with a higher speed limit, and decelerating on a subsequent link with a lower limit. In the second scenario, for short road links, the EV may be unable to reach their maximum speed before needing to decelerate or accelerate for the next segment. This necessitates an adjusted acceleration profile. Fig. 6(b) demonstrates this situation, where the EV does not attain the maximum speed due to the short length of the links. While this model simplifies real-world complexities, it offers an effective approach to the EVRP, aiding in the identification of energy-efficient routes for EVs.

4.4. Charging system

The proposed charging model, illustrated in Fig. 7, captures the nonlinear relationship between SoC, SoH, required charge amount (f), and charging time using a piece-wise planar approximation. Fig. 7(a) shows a 3D surface plot of charging time variation with SoC and SoH, while Fig. 7(b) presents a contour map where offers a clearer view of time changes across different SoH levels. These results underscore the importance of incorporating SoH into decision-making, as it evolves over time and directly impacts charging performance.

4.5. Overview of dynamic framework for aging model

In this section, we present an overview of our proposed dynamic model for SoH estimation, as illustrated in Fig. 8. The framework comprises four main components that iteratively update both the SoC and SoH based on real-time inputs and dynamic conditions. Initially, the road graph and vehicle parameters are utilized to predict the required power consumption at each time step. Subsequently, the battery parameters are updated based on the current SoC and SoH values, with real-time estimation of the six parameters of the battery's equivalent circuit model, ensuring accurate representation of the battery's evolving state. The power consumption, along with the updated battery parameters, is input into the battery model, which also considers voltage, current, SoC, and SoH to compute the SoC for the subsequent time step. The resulting SoC profile is then analyzed by the degradation model, which decomposes the SoC trajectory into equivalent stress cycles. Based on each cycle's amplitude, mean value, and temperature, the degradation model estimates the SoH. Each update is synchronized with the sampling interval T_s.

5. Optimization method

Our problem involves mixed-integer and continuous decision variables and requires calculating SoC at each time step and applying

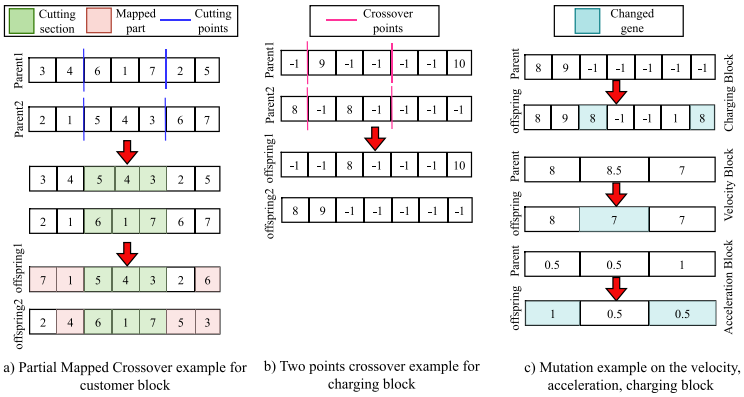

Fig. 9. Illustrative example of genetic operators on chromosome blocks: (a) partial-mapped crossover (PMX) on the customer block; (b) two-point crossover on the charging block; and (c) mutations applied to the velocity, acceleration, and charging blocks.

rainflow counting for SoH, yielding a nonconvex and expensive objective. To address this, we adopt GALS) to efficiently solve the objective function in Eq. (4). the GA provides global exploration of the solution space, while the LS performs local refinement of the GA solution. Fig. 10 depicts the EVRP-AFM solution derived via a GA that integrates both direct and indirect route representations. Each chromosome encodes the complete solution for all EVs and is decoded into sub-chromosomes corresponding to individual vehicles. The mission plan defines the EV's route, specifying the sequence of customers and CSs to be visited. It consists of two main components: the customer block and the charging plan block.

The customer block is a vector of integers, N', listing the customers assigned to the EV. The charging plan block specifies the charging stations C' the EV will visit and the corresponding charge amounts f at each station. Each mission plan is encoded as the stacked tuple sequence $((N'_0, C'_0, f_0), \ldots, (N'_m, C'_m, f_m))^T$, where N'_i is the ith customer, C'_i the charging station after N'_i (with C'_i=−1 meaning no stop at charging station), and f_i the corresponding charge. After the GA optimization finishes, LS starts from the GA's current best solution and explores a swap-based neighborhood on the customer block. LS generates all pairwise swaps of customer positions (other chromosome parts are kept unchanged), evaluates each neighbor with the same cost objective as GA, and moves to the best-improving neighbor. This process repeats until iteration budget is reached, yielding a local refinement of the GA solution.

Algorithm 1 Genetic Algorithm & Local Search (GALS)

Input: mutation prob. P_m; crossover prob. P_c; population size N_{pop}; generations N_{gen}; tournament size k; LS iteration $Iteration$
Output: Current best solution at the last generation

$t \leftarrow 0$; $(X_{\text{best}}, f_{\text{best}}) = (None, \infty)$; $\mathcal{P}(t) \leftarrow$ InitPopulation(N_{pop})
for each $X \in \mathcal{P}(t)$ **do** $f(X) \leftarrow$ Evalution(X) ▷ Alg. 2
while $t < N_{\text{gen}}$ **do**
  $\mathcal{P}_{\text{parent}} \leftarrow$ Select($\mathcal{P}(t)$, k)
  $\mathcal{P}_{\text{offspring}} \leftarrow$ Crossover($\mathcal{P}_{\text{parent}}$, P_c)
  $\mathcal{P}_{\text{offspring}} \leftarrow$ Mutate($\mathcal{P}_{\text{offspring}}$, P_m)
  for each $X \in \mathcal{P}_{\text{offspring}}$ **do** $f(X) \leftarrow$ Evaluation(X) ▷ Alg. 2
  $\mathcal{P}(t+1) \leftarrow$ Update($\mathcal{P}_{\text{offspring}}$, $\mathcal{P}(t)$)
  $(\tilde{X}, \tilde{f}) \leftarrow \left(\arg\min_{X \in \mathcal{P}(t)} f(X), \min_{X \in \mathcal{P}(t)} f(X)\right)$
  if $\tilde{f} < f_{\text{best}}$ **then**
    $(X_{\text{best}}, f_{\text{best}}) \leftarrow (\tilde{X}, \tilde{f})$
    $t \leftarrow t + 1$
/* —— Local Search —— */
$k \leftarrow 0$; $(X_{\text{cur}}, f_{\text{cur}}) \leftarrow (X_{\text{best}}, f_{\text{best}})$
while $k < Iteration$ **do**
  $\mathcal{S} \leftarrow \mathcal{N}(X_{\text{cur}})$ ▷ build neighbors from $\mathcal{N}$
  $s^\star \leftarrow \arg\min_{s \in \mathcal{S}} f(s)$ **with** $f(s)$=Evaluation(s) ▷ Alg. 2
  if $f(s^\star) < f_{\text{cur}}$ **then**
    $(X_{\text{cur}}, f_{\text{cur}}) \leftarrow (s^\star, f(s^\star))$; $(X_{\text{best}}, f_{\text{best}}) \leftarrow (X_{\text{cur}}, f_{\text{cur}})$

Algorithm 2 Evaluation Function

Input: Chromosome X
Constants: Road graph G_r; weights $\omega_1, \omega_2, \omega_3$; Time sampling interval T_s
Output: Objective value: $f(X)$

/* —— Decode chromosome (by EV IDs) —— */
$(R^*, F^*, t_0^*, V_{\max}^*, a_{\max}^*) \leftarrow$ Decode(X)
for each vehicle z in $\mathcal{Z}$ **do**
  Initialize $SoC^z_{\text{profile}} \leftarrow [\,]$
  for each $(i : R^z_q \rightarrow j : R^z_{q+1})$ in R^z **do**
    Find target velocity V_{tgt} from road graph G_r ▷ Eq. (31)
    for each time step k along (i, j) **do**
      Compute instantaneous power: $P_{\text{mech}}(k)(V_{\text{tgt}}, a^z_{\max}, \theta)$ ▷ Eq. (19)
      Update total mechanical energy: $e^z_{i,j} \leftarrow e^z_{i,j} + P_{\text{mech}}(k)\,T_s$
      Update SoC: $SoC_k \leftarrow$ UpdateSoC(SoC_{k-1}, $P_{\text{mech}}(k)$) ▷ Eq. (26)
      Append SoC_k to SoC^z_{profile}
  Compute degradation: $SoH_z =$ DegradationModel(SoC^z_{profile}) ▷ Eq. (27)–(29)
  Compute arrival time t^z_j and delay D^z_j
/* —— Compute Total Objective Value —— */
$f(X) = \omega_1 \sum_{z \in \mathcal{Z}} \sum_{q=0}^{r^z} D^z_q + \omega_2 \sum_{z \in \mathcal{Z}} \Delta SoH_z + \omega_3 \sum_{z \in \mathcal{Z}} \sum_{q=0}^{r^z} e^z_{R^z_q R^z_{q+1}}$ ▷ Eq. (4)

A pseudo-code of the generic GALS is given in Algorithm 1. A solution encodes, for each vehicle, the assigned customer orders, the visiting paths, the motion dynamics (acceleration and velocity), and the departure times from the depot. We employ a GA to search over such solutions by generating an initial population of chromosomes, where each chromosome represents a complete multi-vehicle plan together with motion parameters and departure times. Each chromosome is scored by an objective that aggregates fleet delay, battery degradation, and energy consumption for the decoded solution (Algorithm 2). The procedure begins by creating the initial population and initializing the best cost, and all individuals in the population are evaluated using the procedure described in Algorithm 2 (Lines 1–2). Parent chromosomes are then selected according to their objective values (Line 4) and used to produce offspring via crossover and mutation (Lines 5–6). We use Partial Mapped Crossover (PMX) for the customer-order block, and a two-point crossover for the remaining sections (e.g., CS choices, charge amounts, departure times, and motion parameters). We introduce diversity by randomly swapping customers, selecting a charging station from $\{-1\} \cup CS$, randomly perturbing the charge amount and departure time, and sampling velocity and acceleration from predefined sets. Fig. 9 illustrates the operators on representative blocks only, (a) PMX on the customer block, (b) two-point crossover on the charging block, and (c) example mutations on the velocity, acceleration, and charging blocks. These blocks are shown as samples to clarify how the operators are applied; in the GA, the same operators are applied to their respective blocks across the entire chromosome. In this illustrative example, we

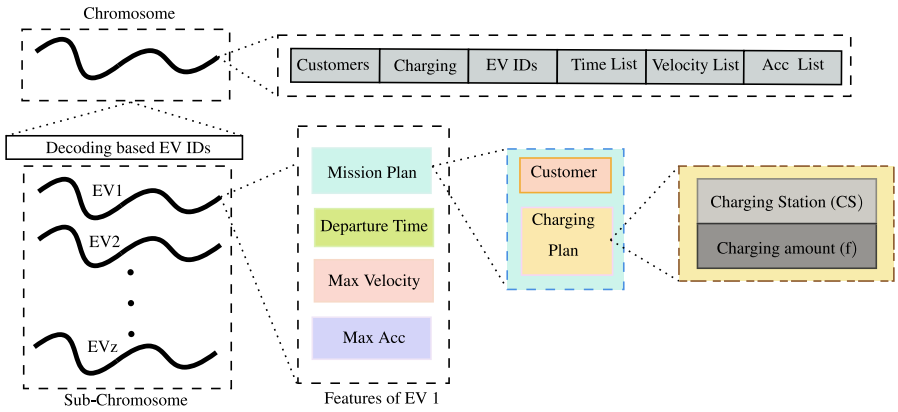

Fig. 10. Representation of a chromosome and its corresponding sub-chromosomes, where each sub-chromosome belongs to a specific EV. The charging plan, reports the ID of CSs and the amount of charge assigned (f).

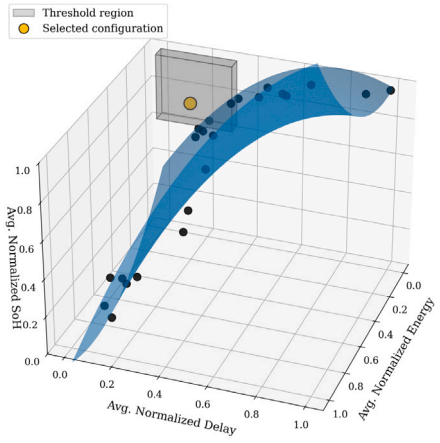

Fig. 11. Variation of normalized energy, delay, and SoH across different weight settings. The yellow point indicates the chosen configuration.

consider 7 customers and 3 CSs served by their EVs. After generating the new offspring, they are evaluated (Line 7), for updating and making new population(Line 8), parents and offspring are merged, all candidates are ranked by their objective cost, and the best individuals are retained for the next generation, so lower-cost solutions persist while higher-cost members are replaced. At each generation, the current best solution is identified by comparison (Lines 9–11). This loop continues until the stopping criterion is met. After GA terminates and returns X_{best}, the LS phase begins. It initializes from the GA best and runs for a fixed number of iterations (Line 15). At each iteration, LS builds the neighborhood from the current solution using the swap structure on the customer block, that is, it generates all pairwise customer exchanges (Line 16). It then evaluates every neighbor with the same objective used in GA and selects the lowest-cost candidate (Line 17). When the candidate improves on the current solution, LS replaces the solution with it and, when applicable, updates the overall best (Line 19). The process continues until the iteration budget is reached, after which the refined best solution is returned.

The evaluation of each chromosome is outlined in Algorithm 2. First, the chromosome is decomposed by EV ID to recover, for every vehicle, its visiting order, charging plan, motion parameters, and departure time (Line 2). Then, for each vehicle encoded in the solution, we simulate its route to assess energy use, battery degradation, and delay; this per-vehicle simulation begins by iterating over the customer visiting order on the route (Lines 3–5). The simulation moves forward in equal time steps between visits, at each time step we compute instantaneous mechanical power from the motion settings and road characteristics, accumulate the corresponding energy, update the SoC, append the new SoC value to the SoC trajectory, and record the timeline needed to derive arrival and delay at the destination (Lines 7–13). The SoC trajectory is analyzed with rainflow counting to obtain the degradation metrics, which are then used to calculate the SoH (Line 12). Finally, across the whole fleet, we aggregate the degradation, energy, and delay terms to produce the chromosome's objective value, which is used as its fitness within the GA (Line 15).

6. Results

A series of numerical experiments were conducted to evaluate the impact of considering battery degradation in routing problems. The experiments were conducted in a synthetic grid environment and real case, generating various instances with different numbers of customers and CSs.

6.1. Experimental setup

To align the optimization process with our application priorities, we define explicit performance thresholds for each objective when selecting weights in the weighted-sum formulation. Energy consumption must not exceed 0.54 kWh, delivery delay must remain below 0.8 h, and the final battery SoH must be at least 0.988. For comparison, the raw values of energy consumption, delay, and SoH are normalized and averaged over multiple experiments so that all objectives are directly comparable, as shown in Fig. 11. In this figure, the predefined thresholds are represented by the gray region; the points within this region satisfy all performance constraints. Among these feasible weights, the yellow point is selected because it yields the highest final SoH. Different ranges of objective values can be achieved depending on application preferences, such as sensitivity to delay, energy consumption, or battery degradation. Based on this analysis, we select $\omega_1 = 2$, $\omega_2 = 0.5$, and $\omega_3 = 1{,}000{,}000$, which satisfy all performance requirements and provide better results in terms of final battery state of health.

The experimental evaluation employed synthetic grid environments to assess the EVRP-AFM method. Each environment was structured as a grid with edges of 1 km. The grid dimensions (in kilometers) were determined by the total number of nodes. All nodes, customers, depot, and CSs, were randomly distributed across the grid. The simulations employed a 250-cell Li-ion battery pack. Table 4 lists the parameters used for the power model and for the optimization. For the mechanical model, we include air density ρ_{air}, aerodynamic drag C_w, rolling resistance C_r, frontal area A, gravity g, and vehicle mass m. For the GALS optimizer, we report the population size N_{pop}, number of generations N_{gen}, crossover probability p_c, mutation probability p_m, tournament

Table 4
Values of mechanical and GALS parameters used in power modeling and optimization.

Mechanical parameter	ρ_{air}	C_w	C_r	A	g	m
Value	1.32 kg/m^3	0.109	0.03	1.2 m^2	9.8 m/s^2	150 kg
GALS parameter	N_{pop}	N_{gen}	p_c	p_m	K	*Iteration*
Value	100	50	0.80	0.60	5	50

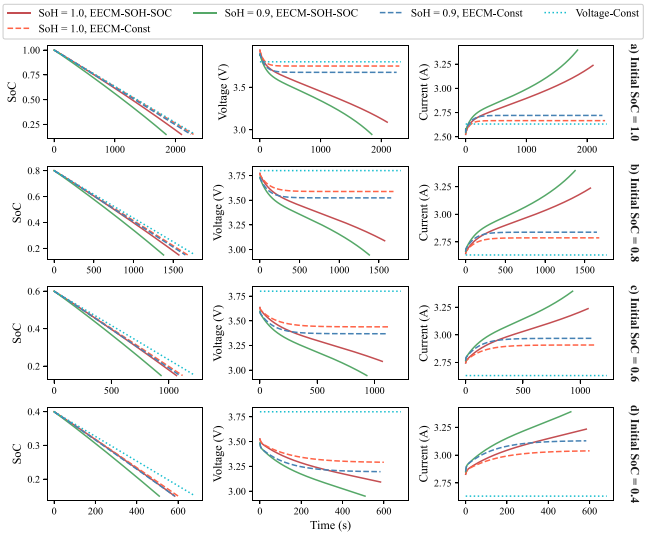

Fig. 12. Comparison of battery models illustrating the influence of SoC and SoH on electrical behavior in new and aged batteries with varying initial SoC states.

size K, and the number of LS iterations (*Iteration*). The experiments were conducted on a machine equipped with an Intel Core i9-13900H CPU (2.60 GHz), 32 GB RAM, running Python 3.11.9 and DEAP v1.4.1. Additionally, we assume that the EVs are fully charged at the beginning of each mission.

6.2. Impact of SoH and SoC on battery dynamics

Modeling battery behavior is essential for calculating the SoC, as it provides a dynamic framework to track and predict battery performance under varying operating conditions. To evaluate our proposed battery model, we compare it with two literature models commonly used in EVRP. For all comparisons, we use an Li-ion battery cell type with a capacity of 2000 mAh. In this section, we assume the vehicle operates at a constant power. The result of this comparison is illustrated in Fig. 12. One of the models included in the comparison is the Voltage Constant model (V-Const), which assumes that the battery voltage is equal to its nominal voltage throughout its operation. This simplifies the analysis by treating voltage as a static parameter. The V-Const is characterized as follows:

$$\mathrm{P}_k^{elec} = \beta \mathrm{P}_k^{mec} \tag{32}$$

$$I_k = \frac{\mathrm{P}_k^{elec}}{V_{nominal}} \tag{33}$$

$$\mathrm{SoC}_{k+1} = \mathrm{SoC}_k - \frac{\eta T_s I_k}{C_{\mathrm{init}}} \tag{34}$$

Another model is the EECM with constant internal battery parameters (EECM-Const), which does not consider the aging effects on model. While it provides a dynamic representation of the battery, it neglects the impact of SoH and SoC on battery's parameters, which is crucial for modeling long-term aging. The EECM-Const is defined as follows:

$$I_k = \frac{-\left(v_k^1 + v_k^2 - V_{\mathrm{OC}}(SoC_k)\right)}{2 \cdot R_s} \pm \frac{\sqrt{\left(v_k^1 + v_k^2 - V_{\mathrm{OC}}(SoC_k)\right)^2 - 4 \cdot R_s \cdot P_k^{elec}}}{2 \cdot R_s} \tag{35}$$

$$v_{k+1}^1 = \left(1 - \frac{T_s}{R_1 C_1}\right) v_k^1 + \frac{T_s}{C_1} I_k \tag{36}$$

$$v_{k+1}^2 = \left(1 - \frac{T_s}{R_2 C_2}\right) v_k^2 + \frac{T_s}{C_2} I_k \tag{37}$$

$$\mathrm{SoC}_{k+1} = \mathrm{SoC}_k - \frac{\eta T_s I_k}{C_{\mathrm{init}} SoH} \tag{38}$$

In Fig. 12, we compare the results of the two models, V-Const and EECM-Const, with our proposed model, EECM-SoC-SoH. For all models, we assume they operate under a constant power condition. Specifically, we evaluate the models for two different initial SoH values: 1.0 (new battery) and 0.9 (degraded battery). Additionally, the initial SoC is varied from 1.0 down to 0.4, with steps of 0.2. In each of the subplots, we observe the evolution of three electrical quantities over time: SoC, voltage, and current.

For the EECM-Const model, we determine the fixed battery parameter values based on the initial SoC and SoH using Eq. (21), and V-Const considers the terminal voltage and the currents remain constant. Additionally, for calculating the Voc, we use Eq. (20).

By examining the trends in voltage, current, and SoC, the results illustrate how the EECM-SoC-SoH model differs from the other models by considering the effects of both SoC and SoH on internal battery parameters. Notably, the EECM-SoC-SoH model reveals that as the battery's SoH declines, indicating degradation, the charge depletes more rapidly. This underscores the significant impact of SoH on battery performance over time.

As batteries age, their internal resistance increases, leading to reduced terminal voltage under load. To maintain power output, systems draw higher current. Our EECM-SoC-SoH model captures this behavior by updating parameters in real-time to reflect the battery's aging state, as demonstrated in Fig. 12. Our battery model, based on our previous work (Heydarzadeh et al., 2023), shows that by considering the aging effect on the model parameters, the proposed model can obtain a more accurate SoC value, with SoC estimation errors remaining under 2%.

6.3. Optimization validation

This section compares the effectiveness of our proposed algorithm (GALS) with other optimization methods in solving the EVRP-AFM, measured by both execution time and objective cost. We examine several established techniques for decision-making and routing problems: GA (Longhitano et al., 2024), Particle Swarm Optimization (PSO) (Kuo et al., 2023), Brute Force Algorithm (BFA) (Saxena et al., 2019; Violina, 2021), Adaptive Large Neighborhood Search (ALNS) (Erdelić et al., 2025), and LS (Cuervo et al., 2014). Conventional Mixed-Integer Linear Programming (MILP) solvers were excluded from this comparison, as they are not subtile for the nonlinear, non-convex optimization problem posed by our dynamic battery model. Their application would demand simplification of the battery dynamics, contradicting a key contribution of this work.

The parameter configurations for each algorithm are detailed in Table 5. We systematically explored the GA and GALS parameters to select suitable values for the experiments. Specifically, the crossover and mutation probabilities for GA and GALS were tested at multiple values: 0.2, 0.4, 0.5, 0.6, 0.7, 0.8, and 0.9. For each combination, we executed the algorithm multiple times and recorded the average objective values. Based on this analysis, the crossover probability was set to 0.8 and the mutation probability to 0.6 for both GA and GALS. All algorithms are tested across six different random environments, with the number of customers and environment size for each environment

Table 5
Parameter settings for each algorithm.

Parameter	GALS	PSO	GA	LS	ALNS
Population size	100	100	100	–	–
Generations/Iterations	50	100	100	150	500
Crossover probability	0.8	–	0.8	–	–
Mutation probability	0.6	–	0.6	–	–
Inertia weight (w)	–	0.8	–	–	–
c_1, c_2	–	0.5, 0.3	–	–	–
Destroy/Repair operators	–	–	–	–	4/3
Operator weights (w_0^o)	–	–	–	–	1.0
Weight update factor (ρ)	–	–	–	–	0.1
Score parameters (σ_1, σ_2, σ_3)	–	–	–	–	(3, 2, 1)
Update interval	–	–	–	–	50

Table 6
Description of the six test environments used for comparing optimization algorithms.

Environment	Number of customers	Environment size (km)
Env1	2	1 × 1
Env2	4	2 × 2
Env3	6	2 × 2
Env4	8	2 × 2
Env5	15	3 × 3
Env6	24	4 × 4

depicted in Table 6. To reduce complexity, CSs are not considered in these environments.

Fig. 13 presents the results comparing the optimization algorithms. In small problem environments such as Env. 1, all methods demonstrate close effectiveness in both objective cost and execution time, but their performance diverges as the number of customers increases. The BF method guarantees an optimal solution for smaller instances (Env. 1–4) but becomes computationally prohibitive, and therefore impractical, for environments with a large number of customers (Env. 5,6). While PSO starts well, it loses efficiency in larger environments compared to other population-based methods, like GA and ALNS. LS, a single-solution approach, is fast for small scales but suffers in solution quality and runtime for larger problems due to limited exploration (Env. 3–6). The GA maintains diversity through its operators, allowing it to outperform PSO in larger environments and even surpass ALNS in (Env. 2–4). ALNS itself proves highly efficient in large environments due to its effective destroy-and-repair mechanism. Ultimately, the GALS achieves the best overall fitness by combining global exploration with local refinement, particularly excelling in the largest environments. This comparative analysis allows us to evaluate these alternative methods and select the most suitable approach. Consequently, we choose the GALS as the primary solver for EVRP-AFM problem.

6.4. Impact of considering aging

We conducted experiments across various environments to analyze the impact of different cost function criteria on solving the EVRP-AFM. We investigated how variations in cost functions influence the resulting mission plans and examined the effect of incorporating aging into the optimization process on routing decisions.

The optimization is evaluated using four different cost function criteria:

- **QoS-Aware (QoS-A):** Prioritizing customer satisfaction by ensuring all demands are met within the specified time windows ($\omega_2, \omega_3 = 0$).
- **Energy-Aware (EA):** A classic EVRP approach that focuses on minimizing the vehicle's overall energy consumption, without considering customer satisfaction or battery degradation ($\omega_1, \omega_2 = 0$).

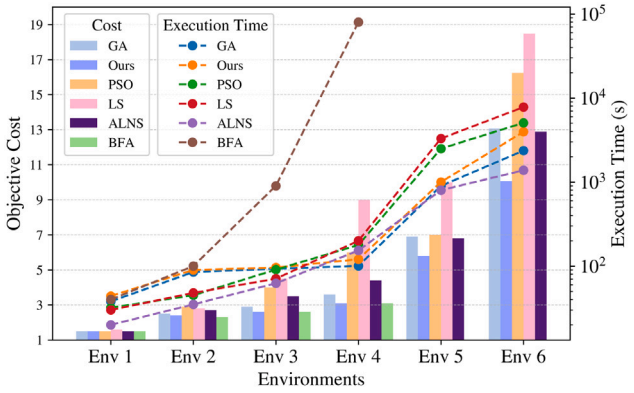

Fig. 13. A comparison of GALS, GA, PSO, LS, ALNS, and BFA in terms of average objective cost and execution time across six environments for EVRP-AFM.

- **Degradation-Aware (DA):** Including battery aging and degradation as key factors in the mission plan to preserve battery health ($\omega_1, \omega_3 = 0$).
- **Multi-Objective-Aware (MOA):** Combining all three criteria, QoS, energy efficiency, and battery preservation, for a balanced approach.

In Table 7, we present the optimized mission routes for various EVRP-AFM instances. These instances are generated randomly in a grid-based synthetic environment. Instance 1 includes 12 customers and 3 CSs, Instance 2 includes 15 customers and 5 CSs, and Instance 3 includes 20 customers and 4 CSs. Each route begins and ends at the depot, denoted by zeros, with CSs highlighted in red along the path. This table demonstrates how different cost functions influence the optimized routes, resulting in distinct paths for each scenario. To evaluate optimized routes, Fig. 14 presents the outcomes derived from Table 7, evaluating how different cost functions affect SoH, energy consumption, travel delays, and cost. Fig. 15 shows the optimized mission plans for Instance 1. Additionally, Fig. 16 illustrates the charging plans and SoC profiles for the optimal mission plan in Instance 1 under different optimization criteria. As shown, In the case of QoS-A, the mission plan is shorter, indicating that the vehicle travels at higher speeds. While this reduces delays, it accelerates battery degradation due to increased discharge rates and deeper DoD. Conversely, in the EA scenario, where there are no strict time constraints, the EV can visit CSs if they are located along the route, rather than making additional stops. However, battery degradation remains high since charging cycles still induce stress on the battery. In the DA scenario, routing mitigates battery wear by keeping mechanical power modest and limiting unnecessary charging events, which yields a smoother SoC trajectory and better long-term battery health. The MOA balances delay, energy use, and battery preservation.

On average, MOA reduces costs by 19% compared with other optimization criteria in Instance 1, 23% in Instance 2, and 21% in Instance 3. These results demonstrate that multi-objective optimization effectively improves cost-efficiency while maintaining sustainable battery health over extended operations.

6.5. Impact of dynamic vehicle constraints

In this section, we show how optimizing motion-related decision variables, such as speed and acceleration, can impact long-term battery health. We call this approach Dynamic Vehicle Control (DVC), which adjusts the vehicle's speed and acceleration to optimize its motion. Table 8 presents experimental results for scenarios with a random number of customers and charging stations, comparing cases with and

Table 7
Optimized routes considering different optimization criteria in various environments. CSs along the route are highlighted in red, and the route starts and finishes at the depot.

Instance	#Customers	#CSs	Environment size	QoS-A	EA	DA	Route
1	12	3	3 km × 3 km	✓			0, 9, 7, 3, 4, 2, 6, 12, 5, 11, 8, 1, 10, 0
					✓		0, 1, 8, 11, 5, 12, 3, 9, 15, 10, 6, 7, 2, 4, 0
						✓	0, 1, 8, 2, 11, 5, 12, 9, 3, 7, 6, 4, 10, 0
				✓	✓	✓	0, 8, 5, 9, 3, 4, 7, 2, 1, 11, 12, 6, 10, 0
2	15	5	4 km × 4 km	✓			0, 5, 11, 13, 3, 14, 10, 7, 6, 8, 15, 2, 9, 12, 1, 4, 0
					✓		0, 6, 11, 16, 8, 3, 15, 12, 1, 4, 9, 2, 7, 13, 14, 5, 10, 0
						✓	0, 8, 11, 1, 6, 3, 15, 12, 9, 2, 10, 7, 4, 13, 14, 5, 0
				✓	✓	✓	0, 5, 6, 11, 3, 8, 12, 15, 1, 4, 10, 14, 13, 7, 2, 9, 0
3	20	4	4 km × 4 km	✓			0, 3, 17, 20, 4, 9, 13, 12, 14, 5, 19, 1, 15, 16, 8, 6, 10, 7, 2, 11, 18, 0
					✓		0, 13, 14, 5, 20, 10, 16, 19, 23, 18, 3, 8, 17, 7, 2, 9, 12, 15, 1, 4, 11, 6, 0
						✓	0, 20, 11, 16, 19, 8, 15, 2, 9, 1, 4, 17, 12, 18, 13, 10, 7, 14, 5, 6, 3, 0
				✓	✓	✓	0, 4, 17, 9, 20, 5, 18, 3, 19, 15, 1, 6, 11, 8, 16, 12, 2, 7, 10, 13, 14, 0

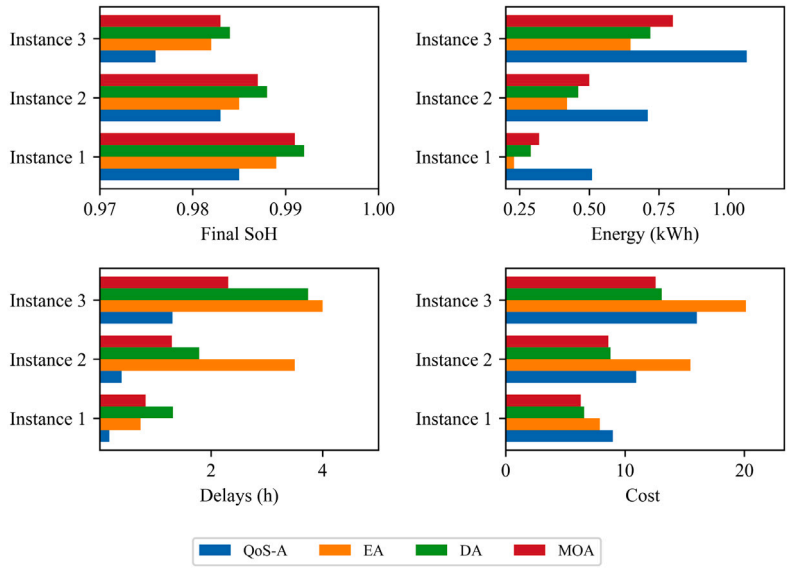

Fig. 14. Results for EVRP-AFM considering different optimization criteria (QoS-Aware: QoS-A, Energy-Aware: EA, and Degradation-Aware: DA). Three instances are presented for each condition. The final SoH is recorded after the electric vehicle traverses the optimal route 1000 times.

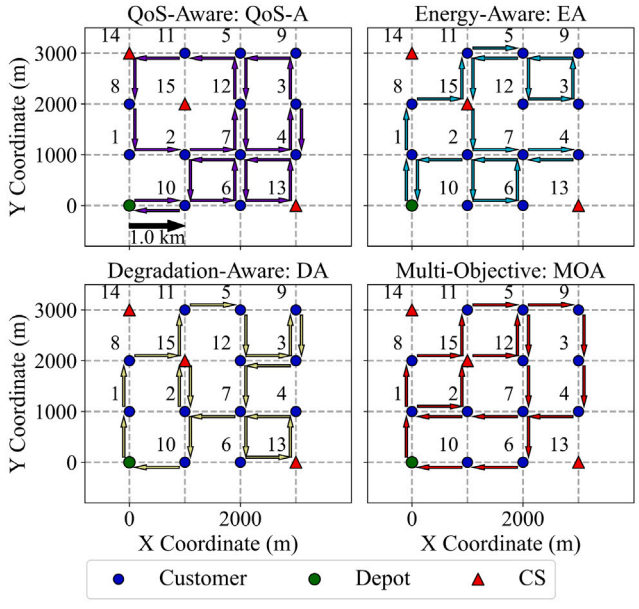

Fig. 15. Optimized routes for different cost function for Instance 1.

without DVC. In the first scenario, without DVC, the vehicle operates at the maximum speed allowed by road conditions. In the second scenario, DVCs are applied as detailed in Section 4.3. According to the results, applying DVC reduces costs and extends battery life, particularly in complex environments. By limiting maximum speed and acceleration, DVC decreases energy consumption and mitigates battery aging. Fig. 17 shows the battery SoH and SoC profiles for the optimal route decisions with and without DVC, based on the two scenarios in Table 8 with 20 customers and 4 CSs, and 30 customers and 10 CSs. As shown in Fig. 17(b) and (d), DVC produces a smoother SoC profile, resulting in gradual decreases and reducing the need for frequent charging cycles. This approach minimizes partial charging events, further preserving battery health.

In Fig. 17(d), for the scenario with more customers, the EV requires charging due to the SoC threshold. However, with DVC, charging frequency is reduced, whereas without DVC, the SoC depletes faster, causing more frequent charging cycles. Charging occurs at approximately 31% SoC without DVC compared to 36% with DVC. The deeper DoD without DVC introduces more stressful cycles, accelerating battery degradation over time. Fig. 17(a) and (c) illustrate battery degradation after traversing the optimal route 1000 times. For 20 customers, 4 CSs, using DVC improves battery health by approximately 44.8%. For 30 customers, 10 CSs, the improvement is about 49%. These results highlight the significant effectiveness of DVC in mitigating battery degradation.

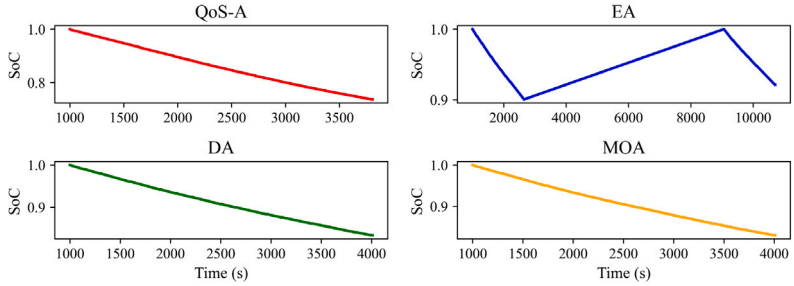

Fig. 16. Comparison of SoC for optimal routes in Instance 1, evaluated across different cost functions.

Table 8
Comparison of experiments conducted with a random number of customers and CSs, showing the final SoH after repeating the optimal path 1000 times and the average cost for traversing the path, with and without Dynamic Vehicle Constraints (DVC).

#Customers	#CS	Environment size	Without DVC		With DVC	
			Avg cost	Final SoH	Avg cost	Final SoH
10	20	5 km × 5 km	10.1	0.988	8.9	0.989
12	12	4 km × 4 km	9.7	0.988	8.6	0.989
20	4	4 km × 4 km	19.3	0.971	12.5	0.984
30	10	6 km × 6 km	86.7	0.922	61.2	0.960

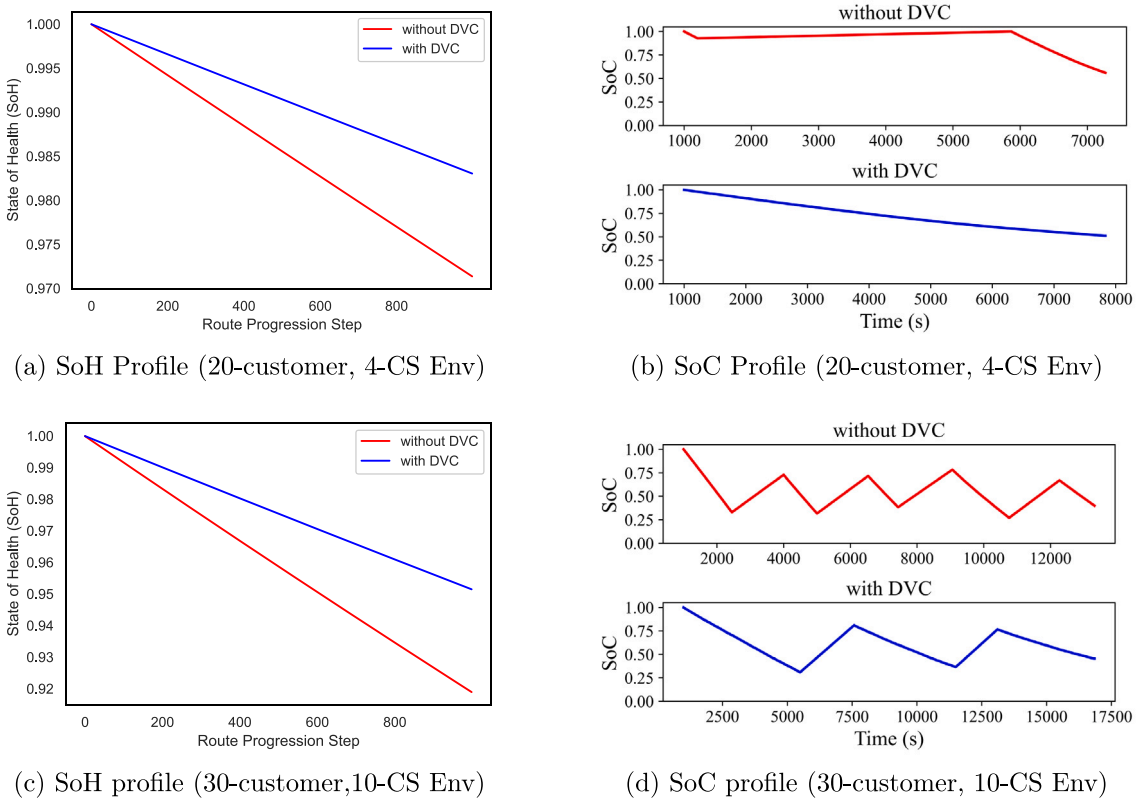

(a) SoH Profile (20-customer, 4-CS Env)

(b) SoC Profile (20-customer, 4-CS Env)

(c) SoH profile (30-customer,10-CS Env)

(d) SoC profile (30-customer, 10-CS Env)

Fig. 17. Comparison of SoH and SoC profiles for the optimal plan of an EV driving with and without Dynamic Vehicle Constraints (DVC). (a) SoH profile illustrating the long-term effects of DVC as the EV completes the optimal mission 1000 times in an environment with 20 customers and 4 CSs. (b) SoC profile for the same scenario, showing the charging plan for 20 customers and 4 CSs. (c) SoH profile for a larger environment with 30 customers and 10 CSs, also over 1000 optimal traversals. (d) SoC charging plan for the 30-customer, 10-CS environment. These profiles demonstrate the impact of DVC across different grid scales and operational conditions.

6.6. Battery lifetime

As observed in previous experiments, incorporating Aging-Aware considerations significantly influences the decision-making variables. This experiment underscores how these considerations shape outcomes over the entire lifecycle, emphasizing their critical role in determining long-term implications. Here, we aim to demonstrate the impact of a Degradation-Aware strategy on the lifespan of the battery. To achieve this, we repeatedly execute the optimized mission plan generated by our GALS in two distinct scenarios: one that optimizes solely based on

Table 9
Comparing battery lifespan with and without Degradation-Aware (DA) optimization across different instances.

#Customer	#CS	Environment size	Lifetime (#Route traversals)		Improvement ratio
			Acting on DA	Not acting on DA	
8	1	3 km × 3 km	28,536	22,257	1.28
12	3	3 km × 3 km	25,410	17,787	1.43
20	4	4 km × 4 km	11,526	9120[1]	1.26
24	6	5 km × 5 km	6996	5000	1.40
30	10	6 km × 6 km	4655	3789	1.23

customers delay times and energy consumption ($\omega_2 = 0, \omega_3, \omega_1 \neq 0$), and another that additionally incorporates degradation wear into the optimization process ($\omega_2, \omega_3, \omega_1 \neq 0$). We assume that the EV traverses the optimized mission plan daily until the SoH of the battery reaches the specified threshold of 0.8.

Table 9 presents the battery lifetime with and without degradation-aware optimization, measured as the number of times the EV can traverse the optimized route before reaching end-of-life, for various instances with random numbers of customers and CSs. The results highlight the extended battery lifespan achieved through the Aging-Aware optimization approach, with improvements ranging from a ratio of 1.23 to 1.43. By comparing the outcomes of both scenarios, we can clearly see the improvement in battery lifetime when degradation is considered in the optimization process.

6.7. Impact of environment

In this section we want to investigate how different number of customers and CSs, and even the size of environment test can effect on the battery degradation and objectives cost. The availability and placement of CSs are crucial factors, especially in large environments where EVs must recharge to meet SoC constraints. While battery aging directly impacts the optimized mission plan and long-term battery health, other considerations like the distribution and number of CSs also influence these outcomes. As shown in Table 10, an insufficient number of CSs increases the cost and accelerates battery degradation over time. For example, when the number of CSs increases from 6 to 15 for 30 customers, the final SoH improves by 29%, and the objective cost decreases by 14%. Similarly, for 40 customers, increasing the number of CSs from 9 to 23 results in a 17% improvement in SoH and a 39% reduction in cost. These results emphasize the need to account for CS availability in mission planning to enhance battery longevity and reduce costs.

Table 11 illustrates the effect of varying the number of customers while keeping the number of CSs and the environment size fixed. The results show that, within the same environment size, increasing the number of customers leads to higher battery degradation and increased objective cost. For example, in an environment with 20 customers compared to 10 customers, battery degradation increases by 43%, and the objective cost increases by 44%.

To analyze the isolated impact of environment size, the number of customers and CSs is kept constant, and the results are reported in Table 12. It can be observed that as the environment size increases, battery degradation also increases. Specifically, when the environment size increases from 3 × 3 km to 5 × 5 km, battery degradation rises by 38%, and the cost increases by 34%.

6.8. Impact of battery model

Fig. 18 compares the SoH trajectories of two different battery models: one that considers the impact of aging on internal parameters (EECM-SoC-SoH) and another with constant parameters (EECM-Const). Each cycle in the graph represents a single traversal of the mission, with both models following the same route under identical speed and acceleration conditions.

Table 10
Comparison of CS availability in the large-scale environment when the average cost is considered as MOA, with the final SoH recorded after 1000 traversals.

# Customers	# CS	Environment size	Cost	Final SoH
30	6	6 km × 6 km	66.4	0.955
30	10	6 km × 6 km	61.2	0.960
30	15	6 km × 6 km	56.7	0.968
40	9	7 km × 7 km	242.5	0.879
40	15	7 km × 7 km	178.6	0.898
40	23	7 km × 7 km	147.3	0.900

Table 11
Comparison of customer numbers in the environment when the average cost is considered as MOA, with the final SoH recorded after 1000 traversals.

# Customers	# CS	Environment size	Cost	Final SoH
10	3	4 km × 4 km	8.7	0.991
15	3	4 km × 4 km	11.3	0.985
20	3	4 km × 4 km	12.6	0.984

Table 12
Comparison of environment size when the average cost is considered as MOA, with the final SoH recorded after 1000 traversals.

# Customers	# CS	Environment size	Cost	Final SoH
10	4	3 km × 3 km	8.5	0.992
10	4	4 km × 4 km	8.7	0.991
10	4	5 km × 56 km	11.4	0.987

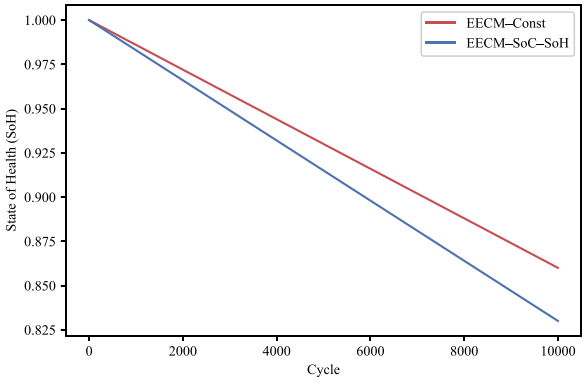

Fig. 18. SoH trajectories comparison: EECM model with constant vs. reconfigurable parameters.

The observed difference in SoH estimations arises from neglecting aging effects on updating the SoC and the battery's parameter model over time. While the initial performance appears similar, the long-term impact of these oversights becomes evident. Over the battery's lifetime, the discrepancy in SoH estimation translates to a difference that represents approximately 1000 mission traversals, underscoring the critical importance of incorporating aging effects into battery modeling.

Fig. 19. Study area in central Helsinki in three real cases, (a) 3 customers, 2 CSs; (b) 5 customers, 3 CSs; (c) 8 customers, 4 CSs. Road network is a grid SUMO map.

Table 13
Comparison of average mission cost and final battery SoH when acting on degradation versus not, in central Helsinki case studies.

#Customers	#CS	Acting on degradation		Not acting on degradation	
		Avg cost	Final SoH	Avg cost	Final SoH
2	2	9	0.991	10.8	0.990
5	3	10.3	0.989	13.6	0.987
8	4	12.5	0.988	15.4	0.985

Table 14
Comparison of average mission cost and final battery SoH with and without Dynamic Vehicle Constraints (DVC), in central Helsinki case studies.

#Customers	#CS	With DVC		Without DVC	
		Avg cost	Final SoH	Avg cost	Final SoH
2	2	9.4	0.990	12	0.988
5	3	11	0.988	14.5	0.986
8	4	13.2	0.987	16.8	0.984

6.9. Realistic use case

To assess the impact of incorporating battery degradation in realistic settings, we consider three EVRP-AFM case studies based on the Helsinki city center map, as shown in Fig. 19. The map is a SUMO grid model of Helsinki that contains real topographical information. The real-world locations of CSs in this area are extracted from map data, while the locations of customers and the depot are generated randomly. The three case studies, depicted in Fig. 19(a), (b), and (c), differ in the number of customers and CSs. Table 13 compares the results obtained with and without accounting for battery degradation. Consistent with the observations on the synthetic network, incorporating degradation leads to better solutions. On average, acting on degradation reduces the mission cost by approximately 20% units across the considered Helsinki case studies. In addition, it results in lower battery wear, with an average reduction in the final SoH loss of about 15% compared to the case where degradation is not considered.

To assess the impact of maximum speed and acceleration in realistic scenarios, an additional set of experiments is conducted. Problem instances are generated and solved both with and without treating speed and acceleration as decision variables. The results, reported in Table 14, show that optimizing speed and acceleration leads to lower mission costs and reduced battery degradation. On average across the three Helsinki case studies, mission costs are reduced by approximately 22%, while battery SoH loss is reduced by about 16%. This improvement is primarily due to reduced energy consumption, which in turn has a positive effect on battery health.

7. Conclusion

This research introduces EVRP-AFM, a new approach to EV routing that recognizes the crucial role of battery degradation into decision-making route planning while imposing constraints on EV behavior. Unlike traditional EVRP models, which often oversimplify battery behavior or neglect real-time parameter updates, EVRP-AFM integrates dynamic battery health as a core element in route optimization. To solve this complex and constraint-heavy problem, a GALS is employed. The approach is validated through comparative experiments, demonstrating its effectiveness in finding optimal solutions. To precisely assess the mission plan's impact on battery health, a cycle-counting model based on the Rainflow algorithm is used. This model examines the SoC history to pinpoint individual cycles and quantify their contribution to battery degradation. By accounting for critical stress factors the model provides an estimate of the degradation accumulated during the mission. Through a series of numerical experiments, we emphasize the importance of using a realistic battery model that dynamically updates the SoC in real time while capturing the evolving behavior of internal battery parameters influenced by aging and SoC. Our results demonstrate that incorporating aging considerations, along with limiting speed and acceleration, significantly extends battery lifespan, offering a robust solution for sustainable fleet management. For future work, we aim to investigate how, in addition to mechanical power, computational power, affected by the complexity of the environment, including factors such as traffic and weather conditions, can influence the aging-aware decision, making problem. This exploration will provide deeper insights into the interplay between environmental dynamics and computational demands in optimizing battery health and operational efficiency.

CRediT authorship contribution statement

Hadis Mohammadi: Writing – review & editing, Writing – original draft, Visualization, Validation, Software, Methodology, Formal analysis, Conceptualization. **Eero Immonen:** Writing – review & editing, Supervision, Conceptualization. **Mohsen Heydarzadeh:** Visualization, Data curation. **Juha Plosila:** Writing – review & editing, Supervision. **Hashem Haghbayan:** Writing – review & editing, Supervision, Conceptualization.

Acknowledgments

This work was supported by funding from the VIREO project, with funders including the European Regional Development Fund (ERDF), Bamomas, and Valmet Automotive, whose contributions are gratefully acknowledged.

Data availability

No data was used for the research described in the article.

References

Agency, I. E. Transport CO_2 emissions. URL https://www.iea.org/.

Ahmed, S., Farhangdoust, S., & Chang, F.-K. (2025). Autoregressive model-based parameter correlation for state of charge and state of health of lithium-ion batteries using built-in piezoelectric transducer induced ultrasonic waves. *Journal of Energy Storage*, *114*, Article 115829.

Azadeh, S. S., Vester, J., & Maknoon, M. (2022). Electrification of a bus system with fast charging stations: Impact of battery degradation on design decisions. *Transportation Research Part C: Emerging Technologies*, *142*, Article 103807.

Barco, J., Guerra, A., Munoz, L., & Quijano, N. (2017). Optimal routing and scheduling of charge for electric vehicles: A case study. *Mathematical Problems in Engineering*, *2017*(1), Article 8509783.

Barré, A., Deguilhem, B., Grolleau, S., Gérard, M., Suard, F., & Riu, D. (2013). A review on lithium-ion battery ageing mechanisms and estimations for automotive applications. *Journal of Power Sources*, *241*, 680–689.

Basso, R., Kulcsár, B., Egardt, B., Lindroth, P., & Sanchez-Diaz, I. (2019). Energy consumption estimation integrated into the electric vehicle routing problem. *Transportation Research Part D: Transport and Environment*, *69*, 141–167.

Braekers, K., Ramaekers, K., & Van Nieuwenhuyse, I. (2016). The vehicle routing problem: State of the art classification and review. *Computers & Industrial Engineering*, *99*, 300–313.

Ceselli, A., Felipe, Á., Ortuño, M. T., Righini, G., & Tirado, G. (2021). A branch-and-cut-and-price algorithm for the electric vehicle routing problem with multiple technologies. *2*, In *Operations research forum* (pp. 1–33). Springer.

Cuervo, D. P., Goos, P., Sörensen, K., & Arráiz, E. (2014). An iterated local search algorithm for the vehicle routing problem with backhauls. *European Journal of Operational Research*, *237*(2), 454–464.

Erdelić, T., Đurasević, M., Erdelić, M., & Carić, T. (2025). Time-dependent electric vehicle routing problem with time windows and charging time dependent on the state of charge. *Computers & Industrial Engineering*, Article 111758.

Fan, L., Liu, C., Dai, B., Li, J., Zhang, Y., & Zhang, R. (2025). An adaptive ant colony algorithm for urban-rural collaborative electric vehicle routing problem. *Applied Soft Computing*, Article 114219.

Froger, A., Jabali, O., Mendoza, J. E., & Laporte, G. (2022). The electric vehicle routing problem with capacitated charging stations. *Transportation Science*, *56*(2), 460–482.

Froger, A., Mendoza, J. E., Jabali, O., & Laporte, G. (2019). Improved formulations and algorithmic components for the electric vehicle routing problem with nonlinear charging functions. *Computers & Operations Research*, *104*, 256–294.

Futalef, J.-P., Muñoz-Carpintero, D., Rozas, H., & Orchard, M. E. (2023). An online decision-making strategy for routing of electric vehicle fleets. *Information Sciences*, *625*, 715–737.

Ghanaee, E., Pérez-Díaz, J. I., Fernández-Muñoz, D., Nájera, J., & Chazarra, M. (2025). Comparative analysis of battery degradation models for optimal operation of a hybrid power plant in the Day-Ahead market. In *2025 IEEE kiel powerTech* (pp. 1–6). IEEE.

Goeke, D. (2019). Granular tabu search for the pickup and delivery problem with time windows and electric vehicles. *European Journal of Operational Research*, *278*(3), 821–836.

Guo, F., Zhang, J., Huang, Z., & Huang, W. (2022). Simultaneous charging station location-routing problem for electric vehicles: Effect of nonlinear partial charging and battery degradation. *Energy*, *250*, Article 123724.

He, Z., Tian, Y., Miao, H., Yao, C., & Yang, Z. (2025). Electric vehicle routing problem with capacitated charging stations and dynamic electricity prices. *IEEE Internet of Things Journal*.

Heydarzadeh, M., Immonen, E., Haghbayan, M. H., & Plosila, J. (2023). A light-weight model for run-time battery SOC-SOH estimation while considering aging. In *ECMS* (pp. 466–472).

Houalef, A.-R., Delavernhe, F., Senouci, S.-M., & Aglzim, E.-H. (2025). Data-driven, personalized route planning for connected electric vehicles: Optimizing time, energy, and charging stops. *Applied Energy*, *402*, Article 126887.

İslim, R. B., & Çatay, B. (2024). An effective matheuristic approach for solving the electric traveling salesperson problem with time windows and battery degradation. *Engineering Applications of Artificial Intelligence*, *132*, Article 107943.

Jung, S. (2025). MILP-based cost and time-competitive vehicle routing problem for last-mile delivery service using a swarm of UAVs and UGVs. *Journal of Air Transport Management*, *124*, Article 102736.

Karakatič, S. (2021). Optimizing nonlinear charging times of electric vehicle routing with genetic algorithm. *Expert Systems with Applications*, *164*, Article 114039.

Kim, Y. J., & Do Chung, B. (2023). Energy consumption optimization for the electric vehicle routing problem with state-of-charge-dependent discharging rates. *Journal of Cleaner Production*, *385*, Article 135703.

König, A., Nicoletti, L., Schröder, D., Wolff, S., Waclaw, A., & Lienkamp, M. (2021). An overview of parameter and cost for battery electric vehicles. *World Electric Vehicle Journal*, *12*(1), 21.

Kuo, R., Luthfiansyah, M. F., Masruroh, N. A., & Zulvia, F. E. (2023). Application of improved multi-objective particle swarm optimization algorithm to solve disruption for the two-stage vehicle routing problem with time windows. *Expert Systems with Applications*, *225*, Article 120009.

Li, R., Kirkaldy, N. D., Oehler, F. F., Marinescu, M., Offer, G. J., & O'Kane, S. E. (2025). The importance of degradation mode analysis in parameterising lifetime prediction models of lithium-ion battery degradation. *Nature Communications*, *16*(1), 2776.

Li, J., Liu, C., Yi, K., Fan, L., & Wu, Z. (2025). An adaptive NSGA-II for electric vehicle routing problem with charging/discharging based on time-of-use electricity pricing and diverse charging stations. *Applied Soft Computing*, *170*, Article 112704.

Li, Q., & Xue, W. (2025). A review of feature extraction toward health state estimation of lithium-ion batteries. *Journal of Energy Storage*, *112*, Article 115453.

Li, S., Zhao, P., Gu, C., Li, J., Huo, D., & Cheng, S. (2022). Aging mitigation for battery energy storage system in electric vehicles. *IEEE Transactions on Smart Grid*, *14*(3), 2152–2163.

Liu, S., Cavalcanti Costa, J. G., Mei, Y., & Zhang, M. (2024). Gpgls: Genetic programming guided local search for large-scale vehicle routing problems. In *International conference on parallel problem solving from nature* (pp. 36–51). Springer.

Liu, Y., Liu, C., Liu, Y., Sun, F., Qiao, J., & Xu, T. (2023). Review on degradation mechanism and health state estimation methods of lithium-ion batteries. *Journal of Traffic and Transportation Engineering (English Edition)*.

Longhitano, P. D., Bérenguer, C., & Echard, B. (2024). Joint electric vehicle routing and battery health management integrating an explicit state of charge model. *Computers & Industrial Engineering*, *188*, Article 109892.

Ma, B., Hu, D., Chen, X., Wang, Y., & Wu, X. (2021). The vehicle routing problem with speed optimization for shared autonomous electric vehicles service. *Computers & Industrial Engineering*, *161*, Article 107614.

Mattson, C. A., & Messac, A. (2005). Pareto frontier based concept selection under uncertainty, with visualization. *Optimization and Engineering*, *6*(1), 85–115.

Montoya, A., Guéret, C., Mendoza, J. E., & Villegas, J. G. (2017). The electric vehicle routing problem with nonlinear charging function. *Transportation Research Part B: Methodological*, *103*, 87–110.

Mrozik, W., Rajaeifar, M. A., Heidrich, O., & Christensen, P. (2021). Environmental impacts, pollution sources and pathways of spent lithium-ion batteries. *Energy & Environmental Science*, *14*(12), 6099–6121.

Mu, G., Wei, Q., Xu, Y., Li, J., Zhang, H., Yang, F., Zhang, J., & Li, Q. (2025). State of health estimation of lithium-ion batteries based on feature optimization and data-driven models. *Energy*, *316*, Article 134578.

Nebuloni, R., Ilea, V., Berizzi, A., Bovo, C., Meraldi, L., Moretti, L., & Raboni, P. (2025). A MILP battery degradation logarithmic model with Real-Time cycle counting calculation. *IEEE Transactions on Industry Applications*.

Pelletier, S., Jabali, O., & Laporte, G. (2018). Charge scheduling for electric freight vehicles. *Transportation Research Part B: Methodological*, *115*, 246–269.

Pelletier, S., Jabali, O., Laporte, G., & Veneroni, M. (2017). Battery degradation and behaviour for electric vehicles: Review and numerical analyses of several models. *Transportation Research Part B: Methodological*, *103*, 158–187.

Perger, T., & Auer, H. (2020). Energy efficient route planning for electric vehicles with special consideration of the topography and battery lifetime. *Energy Efficiency*, *13*(8), 1705–1726.

Romet, P., Tabusse, R., Gechter, F., Aglzim, E.-H., Jemei, S., Bouquain, D., & Chrenko, D. (2021). Autonomous electric vehicle routing problem using ant colony optimization with consideration of the battery state-of-health. In *2021 IEEE 33rd international conference on tools with artificial intelligence* (pp. 475–480). IEEE.

Saner, C. B., Trivedi, A., & Srinivasan, D. (2022). A MILP-based approach to account for battery degradation in electric bus charging scheduling. In *2022 IEEE PES 14th Asia-Pacific power and energy engineering conference* (pp. 1–6). IEEE.

Saxena, R., Jain, M., Malhotra, K., & Vasa, K. D. (2019). An optimized openmp-based genetic algorithm solution to vehicle routing problem. In *Smart computing paradigms: new progresses and challenges: proceedings of ICACNI 2018, volume 2* (pp. 237–245). Springer.

Schiffer, M., Klein, P. S., Laporte, G., & Walther, G. (2021). Integrated planning for electric commercial vehicle fleets: A case study for retail mid-haul logistics networks. *European Journal of Operational Research*, *291*(3), 944–960.

Shehabeldeen, A., Foda, A., & Mohamed, M. (2023). The impacts of battery capacity degradation on optimizing BEBS transit system configuration. In *2023 IEEE transportation electrification conference & expo* (pp. 1–6). IEEE.

Sun, G., Wang, Y., Sun, Z., Wu, Q., Kang, J., Niyato, D., & Leung, V. C. (2024). Multi-objective optimization for multi-UAV-assisted mobile edge computing. *IEEE Transactions on Mobile Computing*.

Tetik Kollugil, E., Sarıca, K., & Topcu, Y. I. (2025). Electric vehicles as an emission mitigation option: expectations and reality. *Clean Technologies and Environmental Policy*, *27*(3), 1093–1114.

Violina, S. (2021). Analysis of brute force and branch & bound algorithms to solve the traveling salesperson problem (TSP). *Turkish Journal of Computer and Mathematics Education*, *12*(8), 1226–1229.

Wang, S., Jin, S., Bai, D., Fan, Y., Shi, H., & Fernandez, C. (2021). A critical review of improved deep learning methods for the remaining useful life prediction of lithium-ion batteries. *Energy Reports*, *7*, 5562–5574.

Wei, X., Niu, C., Zhao, L., & Wang, Y. (2025). Combination of ant colony and student psychology based optimization for the multi-depot electric vehicle routing problem with time windows. *Cluster Computing*, *28*(2), 99.

Xiao, J., Cao, X., Gridley, B., Golden, W., Ji, Y., Johnson, S., Lu, D., Lin, F., Liu, J., Liu, Y., et al. (2025). From mining to manufacturing: Scientific challenges and opportunities behind battery production. *Chemical Reviews*.

Xiao, Y., Zuo, X., Kaku, I., Zhou, S., & Pan, X. (2019). Development of energy consumption optimization model for the electric vehicle routing problem with time windows. *Journal of Cleaner Production*, *225*, 647–663.

Xu, B., Oudalov, A., Ulbig, A., Andersson, G., & Kirschen, D. S. (2016). Modeling of lithium-ion battery degradation for cell life assessment. *IEEE Transactions on Smart Grid*, *9*(2), 1131–1140.

Xu, M., Wu, T., & Tan, Z. (2021). Electric vehicle fleet size for carsharing services considering on-demand charging strategy and battery degradation. *Transportation Research Part C: Emerging Technologies*, *127*, Article 103146.

Yang, B., Ren, T., Yu, H., Chen, J., & Wang, Y. (2025). An evolutionary algorithm driving by dimensionality reduction operator and knowledge model for the electric vehicle routing problem with flexible charging strategy. *Swarm and Evolutionary Computation*, *92*, Article 101814.

Yang, S., Zhang, R., Ma, Y., & Zuo, X. (2025). Adaptive large neighborhood search incorporating mixed-integer linear programming for electric vehicle routing problem with mobile charging and nonlinear battery degradation. *Applied Soft Computing*, *175*, Article 112988.

Yu, K., Yan, P., Liu, Y., Chen, Z., & Kong, X. T. (2025). Battery degradation mitigation-oriented strategy for optimizing e-hailing electric vehicle operations. *Transportation Research Part E: Logistics and Transportation Review*, *196*, Article 104006.

Yuan, Z., Wang, T., Tian, J., Zhang, J., Zheng, J., Wu, J., & Gao, Z. (2026). Mitigate the range anxiety: two-stage optimization for the electric vehicle routing problem with time windows and battery status uncertainty. *Transportation Research Part E: Logistics and Transportation Review*, *205*, Article 104510.

Zang, Y., Wang, M., & Qi, M. (2022). A column generation tailored to electric vehicle routing problem with nonlinear battery depreciation. *Computers & Operations Research*, *137*, Article 105527.

Zeng, Z., Wang, S., & Qu, X. (2022). On the role of battery degradation in en-route charge scheduling for an electric bus system. *Transportation Research Part E: Logistics and Transportation Review*, *161*, Article 102727.

Zhang, D., Dey, S., Perez, H. E., & Moura, S. J. (2017). Remaining useful life estimation of lithium-ion batteries based on thermal dynamics. In *2017 American control conference* (pp. 4042–4047). IEEE.

Zhao, L., Wang, Y., & Cheng, J. (2019). A hybrid method for remaining useful life estimation of lithium-ion battery with regeneration phenomena. *Applied Sciences*, *9*(9), 1890.

Zhou, Y., Lei, Q., Li, L., & Wu, Z. (2025). An overview of energy replenishment strategies for the electric vehicle routing problem: Models and solution algorithms. *Energies*, *18*(23), 6196.

Zhou, Y., Meng, Q., & Ong, G. P. (2022). Electric bus charging scheduling for a single public transport route considering nonlinear charging profile and battery degradation effect. *Transportation Research Part B: Methodological*, *159*, 49–75.